LEGIBILITY NOTICE

A major purpose of the Technical Information Center is to provide the broadest dissemination possible of information contained in DOE's Research and Development Reports to business, industry, the academic community, and federal, state and local governments.

Although a small portion of this report is not reproducible, it is being made available to expedite the availability of information on the research discussed herein.

1

LA-UR-87-2127

CONF-8704118--2

Los Alamos National Laboratory is operated by the University of California for the United States Department of Energy under contract W-7405-ENG-36

LA-UR--87-2127

DE87 011745

TITLE: PION CHARGE-EXCHANGE REACTIONS: THE ANALOG STATE TRANSITIONS

AUTHOR(S): Helmut W. Baer
Los Alamos National Laboratory

SUBMITTED TO: The Proceedings of the 10th INS-KIKUCHI Spring School on Quarks in Nuclei, Shimoda, Japan
April 15-18, 1987

DISCLAIMER

This report was prepared as an account of work sponsored by an agency of the United States Government. Neither the United States Government nor any agency thereof, nor any of their employees, makes any warranty, express or implied, or assumes any legal liability or responsibility for the accuracy, completeness, or usefulness of any information, apparatus, product, or process disclosed, or represents that its use would not infringe privately owned rights. Reference herein to any specific commercial product, process, or service by trade name, trademark, manufacturer, or otherwise does not necessarily constitute or imply its endorsement, recommendation, or favoring by the United States Government or any agency thereof. The views and opinions of authors expressed herein do not necessarily state or reflect those of the United States Government or any agency thereof.

Acceptance of this article, the publisher recognizes that the U.S. Government retains a nonexclusive, royalty-free license to publish or reproduce published form of this contribution, or to allow others to do so, for U.S. Government purposes.

Los Alamos National Laboratory requests that the publisher identify this article as work performed under the auspices of the U.S. Department of Energy

Los Alamos National Laboratory
Los Alamos, New Mexico 87545

MASTER

DISTRIBUTION OF THIS DOCUMENT IS UNLIMITED

PION CHARGE-EXCHANGE REACTIONS: THE ANALOG STATE TRANSITIONS

Helmut W. Baer
Medium-Energy Physics Division
Los Alamos National Laboratory, Los Alamos, New Mexico 87545

ABSTRACT

The general features of pion charge-exchange reactions leading to nuclear-isobaric-analog states (IAS) and double-isobaric-analog states (DIAS), as they have emerged from studies over the past ten years, are reviewed. The energy range investigated is 20 to 550 MeV for IAS transitions and 20 to 300 MeV for DIAS transitions. These data are seen to play an important role in characterizing the pion optical potential, in determining the Δ-N interaction in nuclei, and in the study of nucleon correlations in nuclei. Recent progress achieved in understanding the role of such correlations in double-charge-exchange reactions is reviewed.

I. INTRODUCTION

From the title of this Spring School, "Quarks and Nuclei," one cannot tell whether the organizers believe that there are two separate topics to be covered, "Quarks" and "Nuclei," or whether they are challenging us to link these two topics and to identify phenomena which demonstrate that there are "Quarks in Nuclei." It is true that many nuclear physicists today see the frontier of nuclear physics to be in identifying phenomena whose explanation requires the use of quark degrees of freedom. While this is a goal, it cannot be said it has been accomplished in the domain of nuclear structure physics or nuclear reactions at low-momentum transfers. In my talk there will be one topic—pion double-charge-exchange reactions—where quark degrees of freedom may be relevant. For such reactions, quark models have been invoked to describe the short-range nucleon correlations involved.

It wasn't so long ago—about 15 years—that pion-nucleus reactions were hailed as the new frontier of nuclear physics. Pions were seen to be the "glue" that held nuclei together. It was thought that scattering beams of this glue on nuclei surely would be enlightening. Since about 1975 we've been doing that at the meson factories, mainly LAMPF, SIN, and TRIUMF, but also some at KEK and BNL. We've learned an enormous amount about the phenomenology of pion-nucleus interactions, viz., elastic and inelastic scattering at small and large angles, pion "true" absorption, single and double charge exchange, Δ dynamics in nuclei, and more. From this work we've gotten a fairly good idea of how pions and Δ's interact in nuclei.

While this work was going on, the intellectual focus of nuclear physics was gradually changing. The discovery of the J/ψ resonance in 1974, and the rapid subsequent developments in particle physics had their impact on nuclear physics. Seeing the success of quark models in describing baryon and meson spectra, many nuclear physicists now think it important, even crucial, to find quark signatures in nuclear reactions at medium energies. The real work and creative insights of this endeavor still lie ahead of us. Hopefully this Spring School will provide some inspiration for this task.

A. π-A Scattering

To get an orientation to the subject of pion charge-exchange reactions, it is helpful to examine the generalized level-scattering diagram shown in Fig. 1 for a nucleus with a neutron excess $(N - Z) \geq 2$. Pion reactions are unique in three respects. (1) The pion is the only elementary particle used by nuclear physicists that comes in three states, π^+, π^0, and π^-. This allows for double-charge-exchange (DCX) reactions, which are of interest because they must involve at least two nucleons (or quarks) to conserve charge; in principle they provide a means of studying nucleon-nucleon correlations. (2) The pion is a spin-0 boson. Thus, one has "true absorption" processes $\pi + A \rightarrow A^*$ and "true creation" processes $\pi + A \rightarrow A^* + 2\pi$. These provide prime tools for studying nucleon resonances, such as the $\Delta(1232)$ or $N^*(1440)$, embedded in a nuclear environment. (3) The π-N system has a pronounced, well-isolated resonance, the $\Delta(1232)$, which has spin-3/2, isospin-3/2, and exists in four charge states, Δ^{++}, Δ^+, Δ^0, and Δ^-. This resonance causes π^+ (π^-) scattering between 100 and 250 MeV to occur predominantly on protons (neutrons), thereby giving a pronounced differential sensitivity to neutron vs proton components in nuclear excitations. It also allows for direct observation of isospin mixing in the excited states of $N = Z$ nuclei.

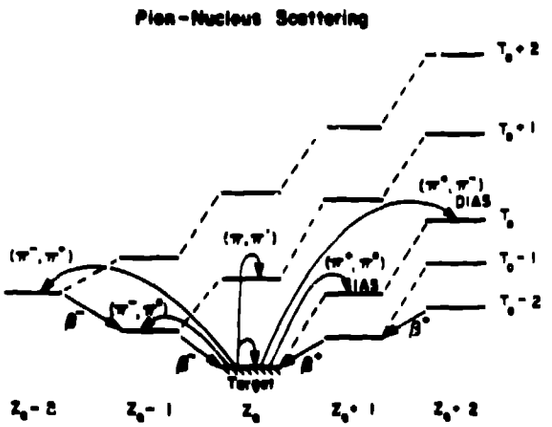

Fig. 1. Generalized level-scattering diagram illustrating the types of scattering phenomena possible with pions.

Of all the states in the spectrum of Fig. 1, two play a special role: the isobaric-analog state (IAS) and the double-isobaric-analog state (DIAS). These states are in the same isospin multiplet as the target ground state and are reached in pion single- and double-charge-exchange reactions. If the target isospin quantum numbers are T and

$T_3 = (N - Z)/Z \equiv T_0$, the IAS has quantum numbers $(T, T_0 - 1)$ and the DIAS has $(T, T_0 - 2)$. These states furnish an excellent opportunity to study single- and double-scattering mechanisms in π-A interactions. In transitions to these states nuclear structure uncertainties are reduced to an absolute minimum because the final states are simply different charge states of the nuclear ground state. Also, in the charge-exchange reactions, Coulomb effects generally play only a minor role, even at low energies, which renders the cross sections directly sensitive to the hadronic interactions. This is unlike elastic scattering, where Coulomb-nuclear interference effects are often quite large. The IAS transitions provide characterization of the single-step scattering mechanism, which forms one part of the double-charge-exchange process. Medium modifications on the elementary $\pi^+ n \rightarrow \pi^0 p$ process, as well as distorted-wave effects in the π-A interaction, can be evaluated on IAS cross sections. This leaves the double-scattering mechanism as the primary phenomenon to be studied in the DIAS transitions. It is these transitions which are unique to pion scattering and which we wish to utilize for investigating nucleon correlations in nuclei and to probe short-range dynamical effects.

B. Examples of IAS and DIAS Transitions

Figure 2 shows the level structure for $A = 14$ nuclei[1] relevant to the discussion of the IAS and DIAS transitions. ^{14}C is the lightest available target for which there is a DIAS transitions.* We see from Fig. 2 that the IAS is an excited state in ^{14}N at 2.31 MeV, and that the DIAS is the ground state of the mirror nucleus ^{14}O. ^{14}C has been a good nucleus for study because of the unusually large level spacings involved, and because of its relatively simple shell structure.[2] Its eight neutrons form a good closed shell and its six protons are in a quite well-determined $(s)^2(p)^4$ configuration.

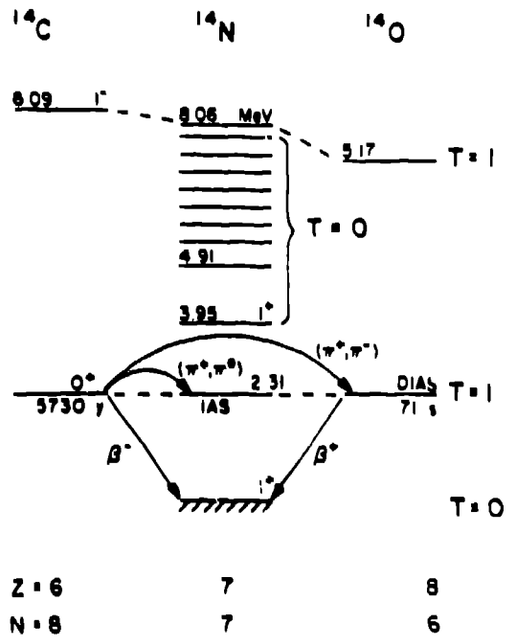

Fig. 2. Level diagram showing the IAS and DIAS transitions on ^{14}C.

*In Los Alamos we have 9 g of radioactive ^{14}C that we have fabricated into a 5- by 5-cm target of thickness 0.3 g/cm^2, and have used for SCX and DCX experiments.

is shown in Fig. 3. The DIAS is expected at an excitation energy of 32.0 MeV in ^{208}Po, based on Coulomb displacement energies.[3] Its isospin is $T = 22$ and it sits in a high density of $T = 21$ and $T = 20$ states. Its natural line width is of considerable interest and can be measured with the DCX reaction, as we shall see below.

Another relevant aspect of IAS and DIAS transitions is that they take place only on the valence neutrons. The probability density distribution $\rho_{\rm val}(r)$ of these neutrons in general does not follow the nuclear matter density $\rho = \rho_n + \rho_p$, which is the sum of neutron (ρ_n) and proton (ρ_p) densities representing all N and Z nucleons, respectively. Figure 4 shows ρ_n, ρ_p, and $\rho_{\rm val}$ for ^{14}C and ^{208}Pb, as obtained from some of the best Hartree-Fock calculations available today.[4] We see that the valence neutrons have very different spatial distributions than ρ_n and ρ_p. In the usual theoretical calculations based on optical potentials, the transition amplitudes for IAS and DIAS transitions are proportional to $\rho_{\rm val}$ and $\rho^2_{\rm val}$, respectively. Thus, these cross sections provide a direct means of studying the valence-neutron density distributions.

C. The Elementary π-N Cross Sections

It is worth taking note of the properties of cross sections of the three elementary π-N processes $\pi^+p \to \pi^+p$, $\pi^+n \to \pi^+n$, and $\pi^+n \to \pi^0p$ involved in IAS and DIAS transitions. (The latter two

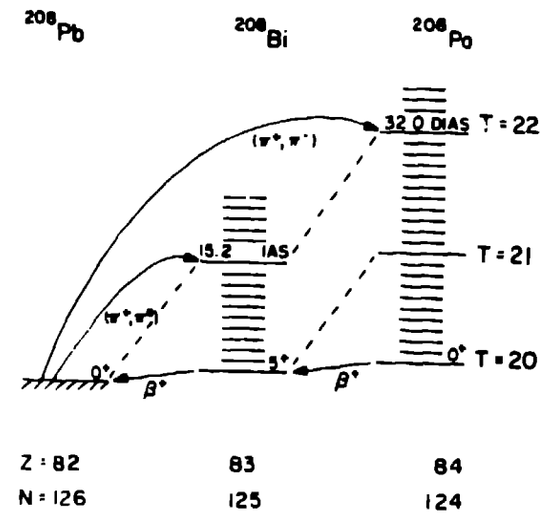

Fig. 3. Illustration of the IAS and DIAS transitions on ^{208}Pb. Both transitions have been measured in pion charge-exchange reactions.

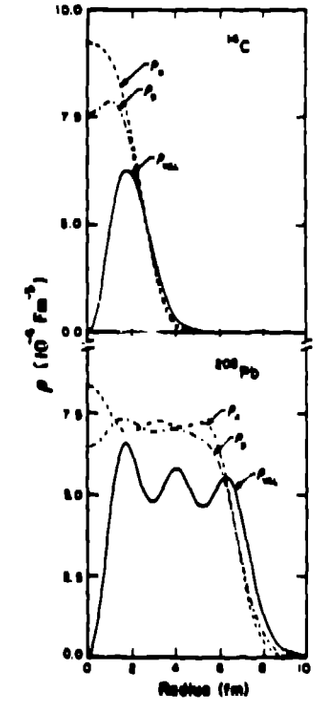

Fig. 4. Density distributions for neutrons (ρ_n), protons (ρ_p), and valence neutrons ($\rho_{\rm val}$) as given by Hartree-Fock calculations (Ref. 4).

are measured in their charge symmetric channels $\pi^- p \to \pi^- p$ and $\pi^- p \to \pi^0 n$.) Figure 5 gives the total cross section for these three reactions from 0 to 1000 MeV. The $P_{33}(1232)$ resonance is the dominant feature and is observed in all channels. The fact that it is quite well isolated from the next highest resonance, the $P_{11}(1440)$, has made it possible to study Δ dynamics, such as Δ propagation and decay, in a relatively well-defined manner. In the energy interval $T_\pi = 300$ to 700 MeV, where recent work has been concentrated, there are the N^* resonances $P_{11}(1440)$, $D_{13}(1520)$, and $S_{11}(1535)$. Unlike the $\Delta(1232)$, these are inelastic resonances which decay a large fraction of the time into $N\pi\pi$, $N\eta$, and $N\rho$ channels (Refs. 7 and 8). The $S_{11}(1535)$ has a particularly large branching ratio ($\simeq$50%) for decay into the $N\eta$ channel, which has been of recent interest.[9]

Total charge-exchange cross sections for $\pi^- p \to \pi^0 n$ and $pn \to np$ reactions are shown in Fig. 6. One sees that the energy dependence of these two cross sections is dramatically different. At low energies $\sigma(\pi^- p \to \pi^0 n) \simeq 0.01\sigma(pn \to np)$. This makes pion charge-exchange reactions on nuclei more tractable in multiple-scattering theories than the (p,n) and (n,p) reactions. It also leads to lower π-A cross sections at energies $T_\pi <$ 100 MeV. At $T_\pi = 180$ MeV, exactly on the $\Delta(1232)$ resonance, the two

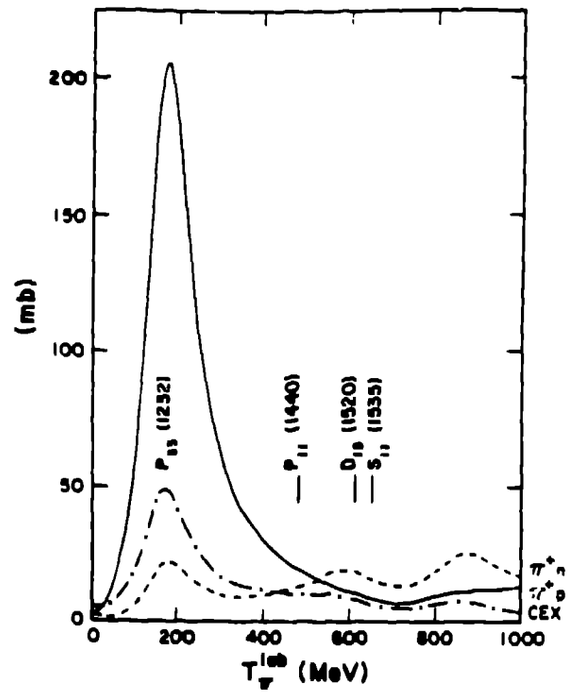

Fig 5. Total cross sections for $\pi^+ n \to \pi^+ p$ and $\pi^+ n \to \pi^0 n$ scattering (Ref. 6). The charge-exchange cross section has been excluded from the $\pi^+ n$ total cross section.

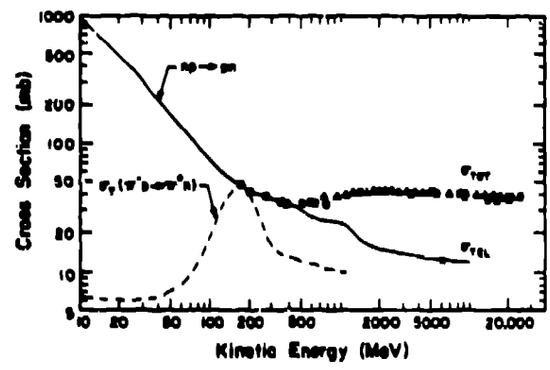

Fig. 6. Comparison of pion and nucleon induced charge-exchange cross sections on a proton target. The np cross sections are from Ref. 10 and the $\pi^- p \to \pi^0 n$ cross sections are from Ref. 7.

processes have equal cross sections with a value of 50 mb.

The angular distributions of the $\pi^- p \rightarrow \pi^0 n$ reaction have some interesting features relevant to IAS and DIAS studies. They are shown for energies 50, 180, and 425 MeV in Fig. 7. At 180 MeV, the angular distribution is nearly symmetric about 90°, a consequence of having nearly pure p-wave scattering, which gives an angular dependence of $(1 + \cos^2\theta)$. This feature was useful in identifying the quantum numbers of the Δ in the early 1950's (Ref. 11). At 425 MeV, and at higher energies, the angular distributions are sharply forward peaked, a feature which makes Glauber models applicable at the higher energies. At 10 MeV (not shown) the angular distribution is nearly isotropic, a consequence of having predominantly s-wave scattering. At 50 MeV the angular distribution is backward peaked, and it has a nearly vanishing cross section at 0°, a consequence of interference in the s and p partial waves. This feature persists in the nuclear scattering and has interesting ramifications for double-charge-exchange scattering, as we shall see below.

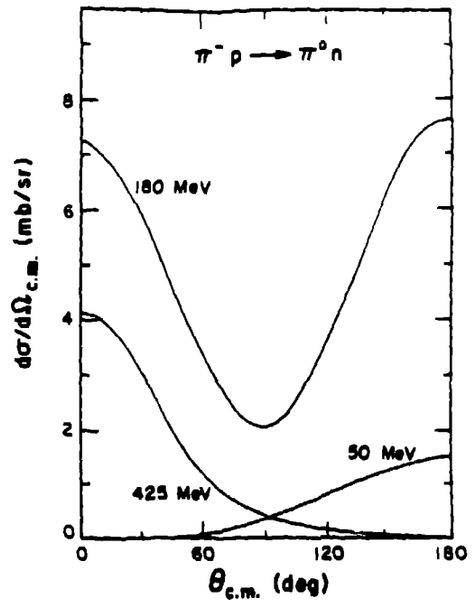

Fig. 7. Angular distributions for the $\pi^- p \rightarrow \pi^0 n$ reactions at three different energies, as given by current phase shift calculations (Ref. 6).

II. PION-NUCLEUS SINGLE CHARGE EXCHANGE

A. π^0 *Spectrometer*

To measure IAS transitions one needs to detect π^0's with an energy resolution commensurate with nuclear level spacings. We have built a π^0 spectrometer[12] in Los Alamos that operates in the resolution range 2 to 5 MeV (FWHM). Figure 8 shows a spectrum measured for the ^{7}Li(π^+, π^0) reaction at 100 MeV. Here we achieved a resolution of 2 MeV (FWHM). Figure 9 shows a recently measured[13,14] spectrum for the $\pi^- p \rightarrow \pi^0 n$ reaction at 425 MeV. The resolution here is 8 MeV (FWHM) of which 6 MeV is the π^0 spectrometer contribution, the remaining coming from beam and target effects. The solid line in Fig. 8 represents the Monte Carlo simulation of the beam, target, and spectrometer. The

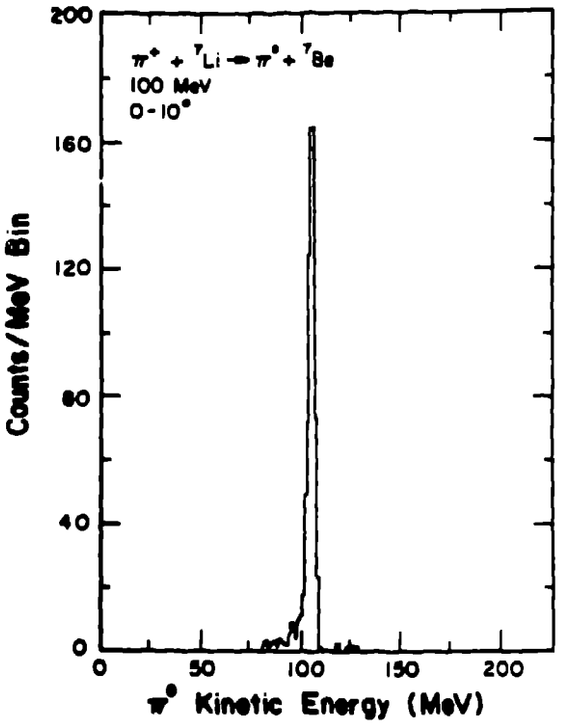

Fig. 8. Spectrum for the ^{7}Li(π^+, π^0) reaction as measured with the LAMPF π^0 spectrometer.

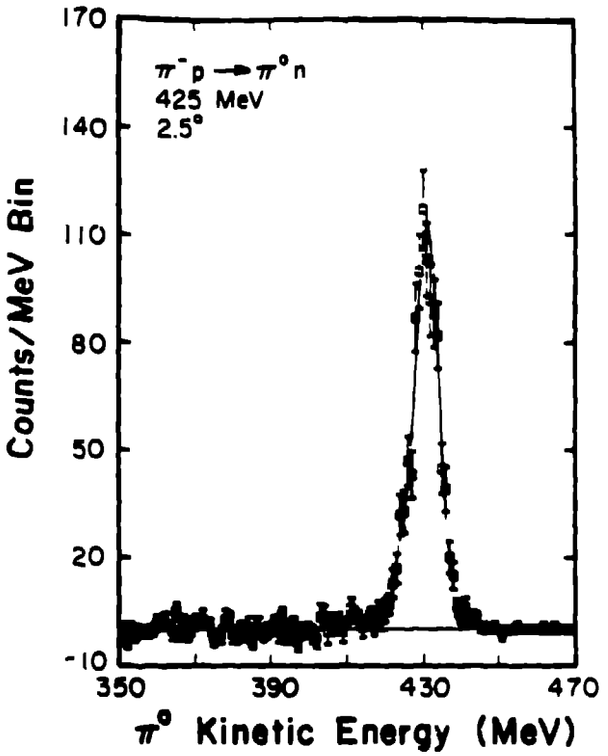

Fig. 9. Spectrum for the $\pi^- p \rightarrow \pi^0 n$ reaction measured with a CH_2 target. A small ^{12}C(π^+, π^0) contribution has been subtracted (Refs. 13 and 14).

measured line shape at this energy as well as other energies is well reproduced by our simulation code.

The spectrometer consists of two large γ-ray detectors used to measure the opening angle and photon energies in the $\pi^0 \rightarrow 2\gamma$ decay. Each detector measures total energy of photons with Pb glass Cherenkov detectors and the γ position coordinate with active Pb-glass converters backed with MWPC's. Each γ detector has three active converters. The distance from the target to the front converter is typically 0.5 m for low-energy measurements (50 MeV) and 2.0 m for the high-energy measurements (425 MeV). A detailed description of the spectrometer is given in Ref. 12.

B. Overview of IAS Transitions

IAS transitions have now been measured by our group in Los Alamos at pion energies from 20 to 550 MeV. Over this interval, the elementary π-N cross sections change enormously, as we have seen. The peak of the Δ resonance occurs[7,8] at 180 MeV incident kinetic energy for the π-N system and its width is 110 MeV (FWHM). In π-A scattering, the peak of the Δ resonance is not so well defined due to binding and A-dependent (e.g., Ref. 15)

effects. The Δ dominance region is generally considered to extend from approximately 65 to 265 MeV. Over this energy region elastic and inelastic scattering angular distributions are sharply diffractive, a feature characteristic of strong absorption. IAS cross sections are also quite forward peaked. Above 300 MeV the π-N total cross sections are relatively flat and small (Fig. 5), and one expects distorted-wave impulse-approximation (DWIA) calculations to work quite well. Below 65 MeV, the character of π-A scattering changes. Pions penetrate into the nucleus and the s-p wave interference puts deep minima in the angular distributions of elastic and charge-exchange scattering. We discuss this energy region separately below.

The first important question answered with the π^0 spectrometer was: does the IAS stand out above the background of other states? This was quite a debated point at the time. We found that it stands out clearly at forward angles. Spectra from our first set of measurements at 98 MeV are shown in Fig. 10. The peaks occurred at the expected energies and the measured cross sections were found to follow the functional form $(N - Z)A^{-4/3}$.

Recently we measured[13,14] the forward angle IAS cross sections for nuclei from ^{7}Li to ^{208}Pb at 425 MeV. Typical spectra are shown in Fig. 11. Again one sees that at forward scattering angles the IAS stands out. The resolution in these data is approximately 8 MeV (FWHM) which makes the extraction of peak areas more problematical. Fortunately, the IAS angular distributions are very sharply forward peaked, and the rest of the spectrum is nearly constant at the forward angles. An overlay of spectra at 1.3 and 5.8° for ^{120}Sn and ^{208}Pb is shown in Fig. 12. The

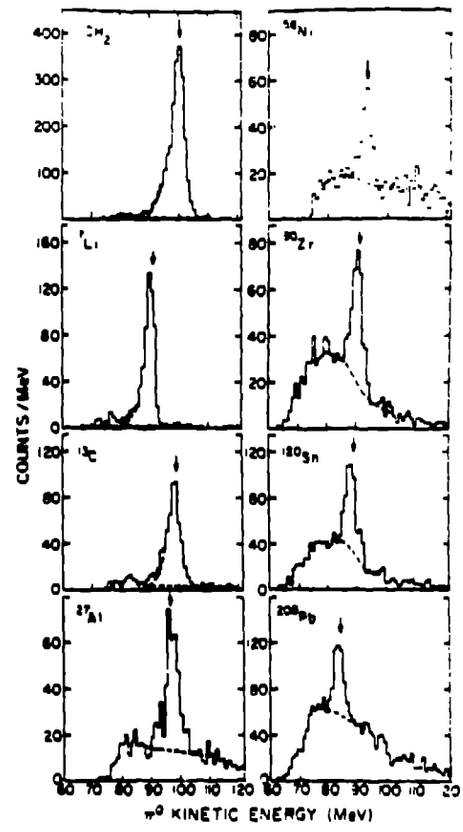

Fig. 10. Spectra measured for the (π^+, π^0) reaction at 98 MeV on various nuclear targets, and for the (π^-, π^0) reaction on a CH_2 target (Ref. 16). The angular range is 0 to 10°.

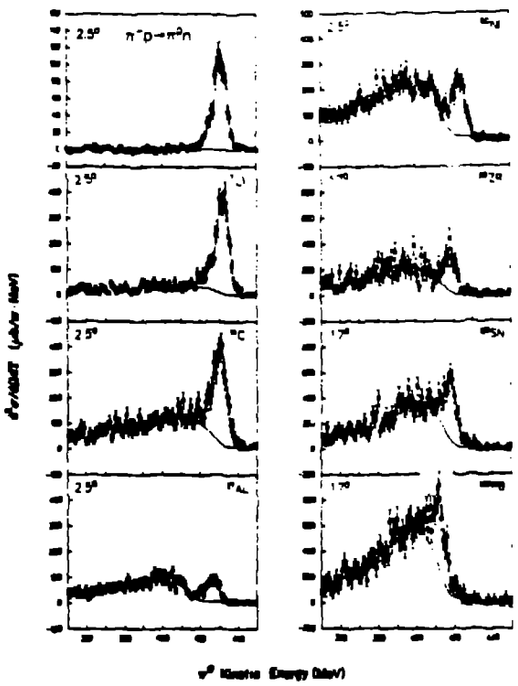

Fig. 11. Spectra measured for the (π^+, π^0) reaction at 425 MeV on various nuclear targets, and for the (π^-, π^0) reaction on a CH_2 target (Refs. 13 and 14).

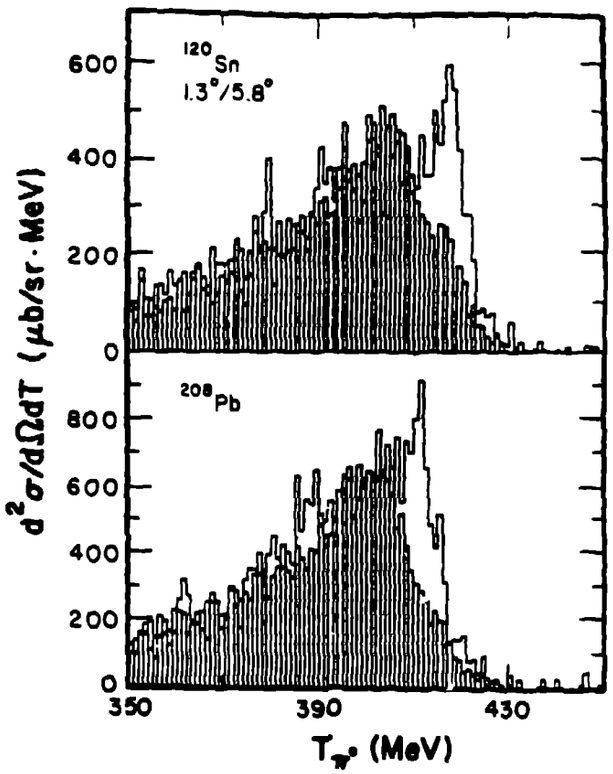

Fig. 12. Overlay of spectra measured at 1.3 and 5.8° for the (π^+, π^0) reaction at 425 MeV on targets of ^{120}Sn and ^{208}Pb (Ref. 14). Only the IAS cross sections are seen to change significantly in this angular interval.

IAS is the only feature of the data which varies significantly. One sees that the IAS peak areas in the 1.3° spectra can be extracted quite reliably, and a good determination of the 0° cross sections can be made.

C. Systematics of IAS Cross Sections, 100 to 500 MeV

The second question addressed in our survey experiments was: do the cross sections exhibit regular patterns with $(N - Z)$ and A, and, if so, over what range of incident energies? If one plots on linear scales the 0° IAS cross section vs A at any energy between 100 and 425 MeV one gets a shape similar to the one shown for 165 MeV in Fig. 13. The function $49(N - Z)A^{-4/3}$ μb/sr, plotted with the data, represents well the overall trend of the data. The factor $(N - Z)$ comes from the fact that the reaction occurs only on valence nucleons. The exponent α in $A^{-\alpha}$ reflects in a qualitative way the degree of pion penetration. A completely transparent disk would give a 0° cross section proportional to

$(N - Z)$; a diffuse black disk leads[18,19] to $(N - Z)A^{-4/3}$. In general, one expects the scattering to be somewhere between these limiting cases, *i.e.*, $0 < \alpha \lesssim 1.33$.

There now exist quite complete data sets at 100, 165, 230, 300, 425, and 500 MeV. The reduced cross section $\sigma(0°)/(N - Z)$ together with power-law fits, are shown in Figs. 14 and 15. The data clearly exhibit a weakening of the A-dependence at higher pion energies, going from $\alpha = 1.34 \pm 0.05$ at 165 MeV to $\alpha = 0.82 \pm 0.10$ at 500 MeV. The experimental values of α are compared to Glauber model values in Table I. From this model we understand the weakened A-dependence to be a consequence of the increased volume scattering at the higher pion energies.

There was a surprising development at $T_\pi > 300$ MeV. The 0° cross sections for all measured nuclei take a big jump between 300 and 425 MeV. The 0° excitation functions for ^{7}Li, ^{14}C, ^{90}Zr, and ^{120}Sn are shown in

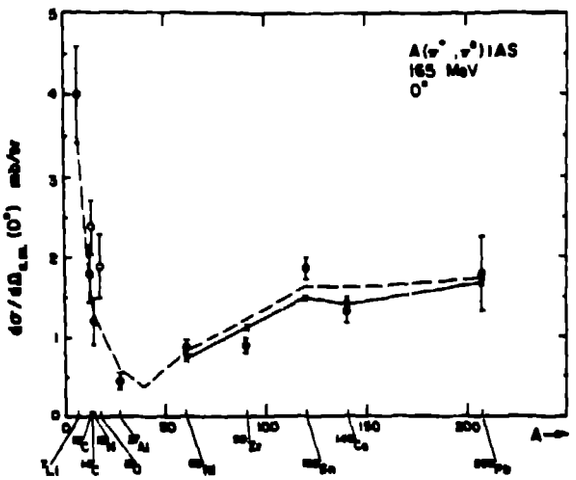

Fig. 13. The dependence on atomic weight (A) of the 0° IAS cross sections at 165 MeV (Ref. 17). The dashed line represents the function 49 $(N-Z)A^{-4/3}$ mb/sr. The solid line represents calculations performed with second-order optical potentials and Hartree-Fock calculations for the neutron and proton density distributions (see Section III.C).

Table I. Values of α obtained from the fits of the expression $(N - Z)A^{-\alpha}$ to the measured 0° IAS cross sections (Refs. 13, 14, and 17) and to the Glauber model values (Refs. 13 and 14).

T_π *(MeV)*	α *Experiment*	α *Glauber Model*
165	1.36 ± 0.04	1.29
300	1.09 ± 0.03	0.93
425	0.94 ± 0.04	0.84
500	0.82 ± 0.10	0.83

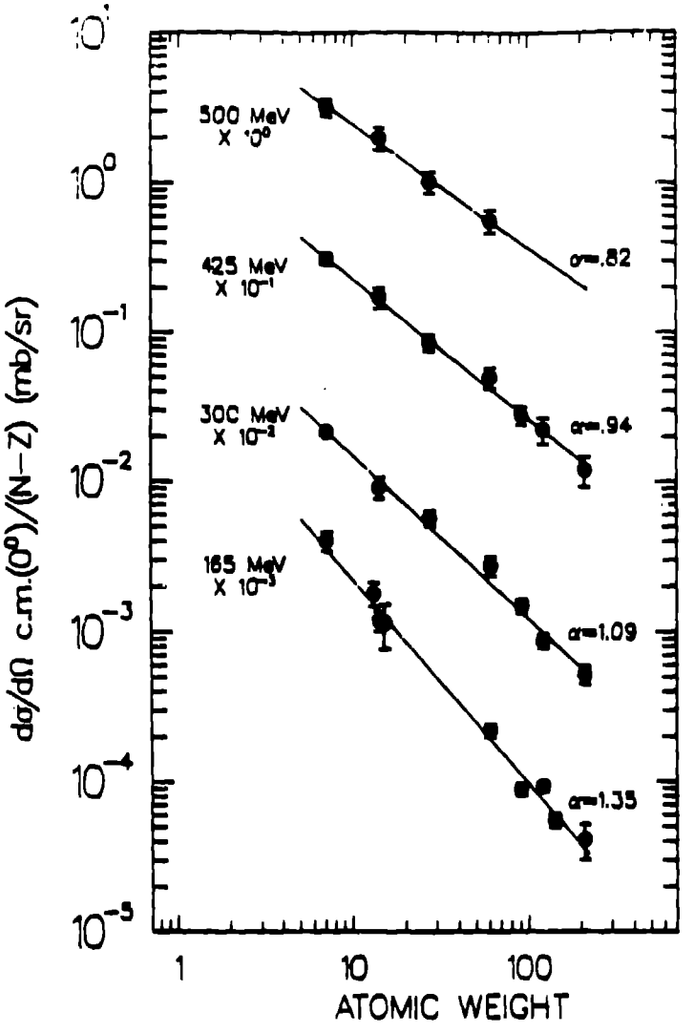

Fig. 14. The A-dependence of 0° cross sections between 100 and 295 MeV. The lines represent fits of the function $g_1(N - Z)A^{-\alpha}$ to the data (Ref. 17).

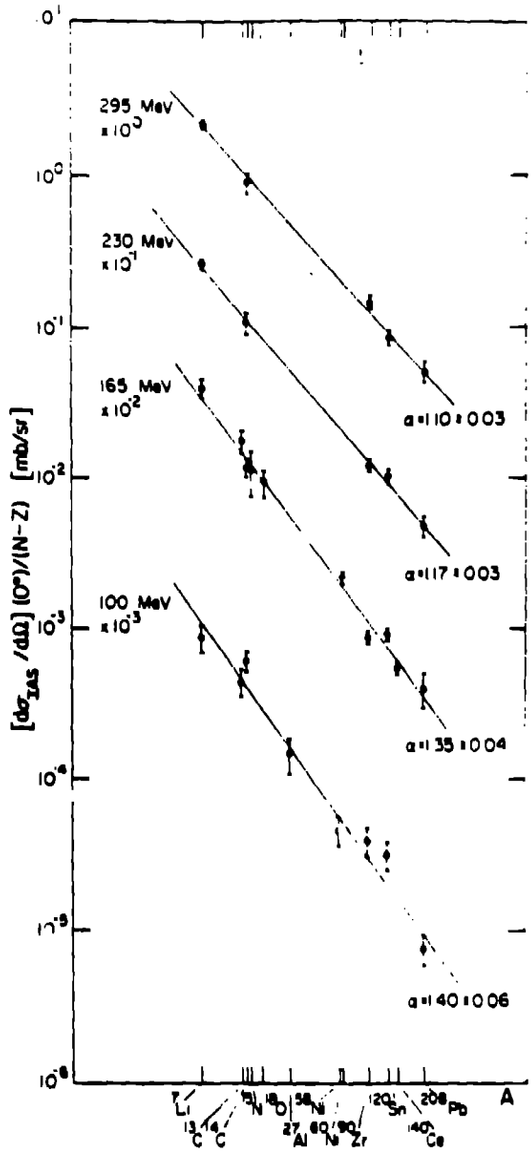

Fig. 15. The A-dependence of 0° cross sections at energies 300, 425, and 500 MeV (Refs. 13 and 14) and at 165 MeV (Ref. 17). The exponent α (defined in Fig. 14) is seen to decrease with increasing energy as expected from increased volume scattering (Ref. 14).

Figs. 16 and 17. This increase by a factor of two or more has forced us to change the way we look at the lower energy data. We used to think that the π-A cross sections follow the trend of the π-N cross sections between 65 and 300 MeV. Now it looks like the π-N cross sections are more properly normalized to the π-A cross sections at 500 MeV or higher energies. When this is done, the excitation functions in π-A scattering exhibit a huge loss of cross section across the Δ region. Thus, the observed shape of $d\sigma/d\Omega_{\rm IAS}(0)$ vs T_π is largely governed by the coupling of the Δ to absorption channels, rather than by the direct $\sigma(\pi$-$N)$ shape. This places strong constraints on theoretical calculations of Δ dynamics.

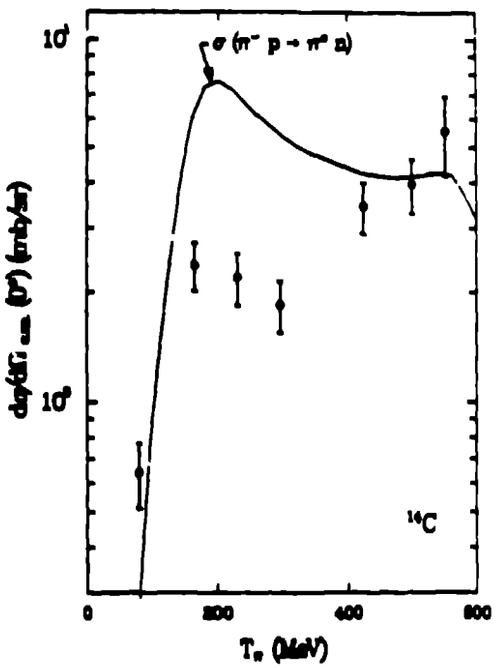

Fig. 16. The energy dependence of the 0° IAS cross sections for ^{14}C (Refs. 13 and 14). The solid line represents the $\pi^- p \rightarrow \pi^0 n$ cross section in the π-N c.m. system vs laboratory kinetic energy.

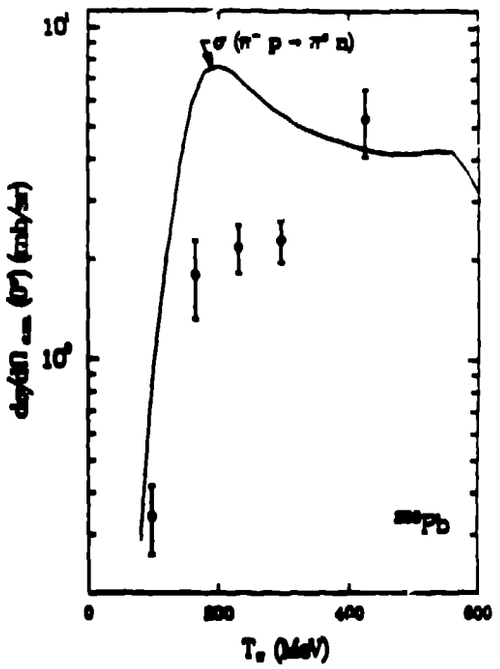

Fig. 17. The energy dependence of the 0° IAS cross sections for ^{208}Pb (Refs. 13 and 14). The solid line represents the $\pi^- p \rightarrow \pi^0 n$ cross section in the π-N c.m. system vs laboratory kinetic energy.

In an attempt to understand qualitatively the origin of the increased cross sections above 300 MeV we carried out an analysis in the framework of the Glauber model for a shadowed single-collision process. Details of the model calculations may be found in Ref. 14. At high pion energies we expect this model to work since the elementary π-N cross sections are relatively weak and the differential cross sections are forward peaked.

Some representative calculations for ^{90}Zr, ^{120}Sn, and ^{208}Pb are shown in Fig. 18. These calculations do indeed predict rising cross sections between 100 and 500 MeV. The data show a step-like increase in cross section between 300 and 425 MeV which the calculations do not reproduce well. The data over the Δ region are not well described by this model.

Our calculations required the use of a phenomenological term to represent higher-order processes such as pion-true absorption. This term has the effect of increasing the attenuation of the pion waves. Without its inclusion, the calculations overestimate the 425-MeV data by a factor of three. As a check on this result, the total reaction cross sections σ_R were calculated and compared to the experimental values at 315 MeV from Ashery *et al.*,[20] which are the highest energy data available. The model reproduces the data quite well, as is seen in Fig. 19. The data and model values may be represented by $\sigma_R = aA^b$ with values $a = 68 \pm 4$ mb and $b = 0.612 \pm 0.002$ for the data, and $a = 49$ mb and $b = 0.69$ for the model.

The high-energy measurements have yielded two significant results: first they showed that there is a large jump in cross section above 300 MeV, a feature which places important new restrictions on theoretical calculations. If indeed this rise is due to increased volume scattering,

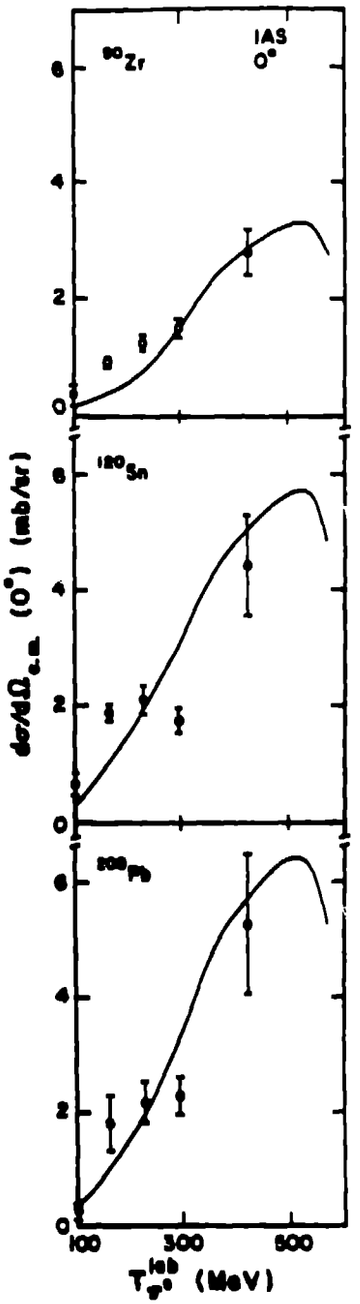

Fig. 18. Comparison of Glauber model calculations (Ref. 14) with measured 0° IAS cross sections for ^{90}Zr, ^{120}Sn, and ^{208}Pb (Refs. 13 and 14). The model calculations included a phenomenological term to represent higher-order processes, such as pion absorption.

it may be expected to be present in many other π-A cross sections. Second, the analysis of the data indicates a sizable role of higher-order effects, such as pion absorption. Thus, it looks like first-order DWIA calculations will not be adequate to describe π-A cross sections at the higher energies, as had been hoped.

D. IAS Transitions, 20 to 80 MeV

At low pion energies the black-disk diffraction scattering picture of π-A scattering must be abandoned. A plane-wave impulse-approximation picture describes the trends of the data much better. The net effect of distortion and pion absorption on the incident and emerging waves seems to be a restoration of the plane-wave picture. The IAS cross section in a plane-wave model[21] is given by (fixed scatterer approximation)

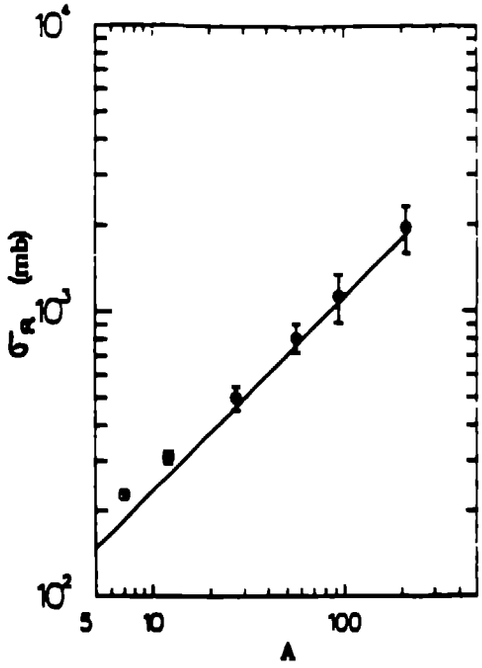

Fig. 19. Total reaction cross sections for π-A scattering at 315 MeV. The data are from Ashery *et al.*[20] The solid line represents Glauber model calculations which were fit to IAS cross sections (Refs. 13 and 14).

$$\frac{d\sigma}{d\Omega}_{\rm IAS}(\pi A) = (N-Z)\frac{d\sigma}{d\Omega}(\pi N)\left|4\pi\int_0^\infty \frac{\sin qr}{qr}\rho(r)r^2dr\right|^2$$

where $d\sigma/d\Omega$ (π-A) and $d\sigma/d\Omega$ (π-N) are the π-nucleus and π-nucleon laboratory cross sections for charge exchange, $\rho = \rho_{\rm val}$ is the valence neutron density, and q is the momentum transfer in the laboratory system. At 0° the quantity in brackets on the right-hand side reduces 1, and we expect the π-A cross section to track directly the π-N cross section. Indeed, this is the case. Figure 20 shows the 0° cross sections for ^{14}C. The ^{14}C data follow closely in shape and magnitude the values of $2\,d\sigma/d\Omega$ (πN) between 34 and 80 MeV. A more detailed analysis reveals that the minimum in the 0° excitation function shifts upward by 4 ± 2 MeV in ^{14}C relative to the free π-N cross section, a result consistent with binding and Pauli blocking effects.

The deep minimum in the IAS excitation function was observed[22] for many nuclei from ^{7}Li to ^{120}Sn. The data are shown in Fig. 21. The curves represent polynomial functions that were fit to the data to locate the position of the minima. The persistence

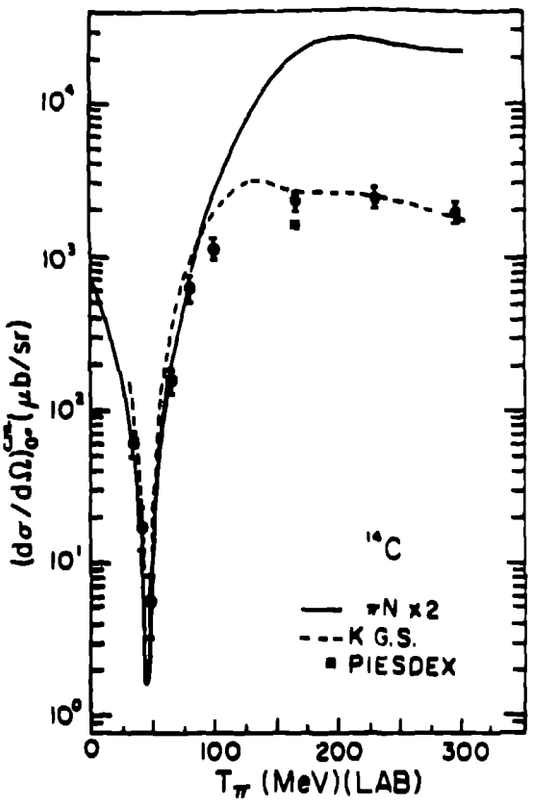

Fig. 20. The energy dependence of 0° IAS cross sections on ^{14}C (Ref. 21). The solid line represents two times the free $\pi^- p \rightarrow \pi^0 n$ cross section. The dashed line represents the multiple scattering theory calculations of Kaufmann *et al.* as discussed in Ref. 21.

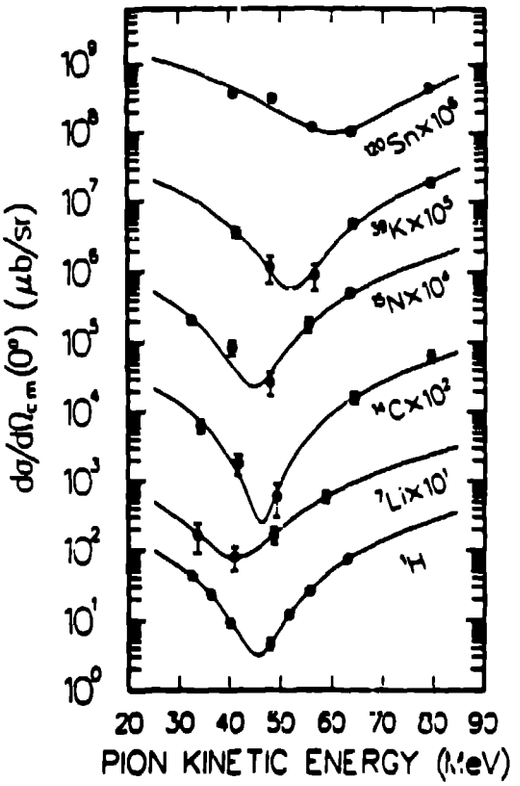

Fig. 21. The measured 0° excitation functions for the IAS transition at low pion energies.[22]. The solid lines represent polynomial fits to the data used to determined the energy of the minimum cross sections.

of the sharp dip structure in nuclear scatterings puts strong constraints on any proposed medium effects. Certainly this deep dip could have been substantially wiped out if multiple scattering and absorption effects were appreciable. This important result obtained from the low-energy IAS measurements allows one to proceed with greater confidence in the analysis of low-energy DCX scattering.

We note here that the measurements[23] at 20 MeV for IAS transitions in ^{7}Li, ^{14}C, ^{15}N, and ^{120}Sn were recently completed. When these new lowest-energy data are added to the 0° excitation functions, one sees that they continue to follow the trend of the free charge-exchange cross sections. Also, an evaluation of Coulomb effects showed them to be small, even at this low energy.

III. PION DOUBLE-CHARGE-EXCHANGE REACTIONS IN THE Δ-RESONANCE REGION

A. *Overview*

It again makes sense to discuss the 100 to 300 MeV region separately because strong absorption and Δ dynamics play such a large role at these energies, whereas at low energies other effects dominate. The low-energy results are discussed in Section IV.

There are some experimental aspects of measuring IAS and DIAS transitions worth noting. Forward-angle IAS cross sections are of order mb/sr, whereas forward-angle DIAS cross sections are of order μb/sr. The actual data accumulation rates per measured cross section have been not so different because (π^+, π^0) cross sections were measured with a solid angle typically 10^{-3} sr and with an incident flux of 5×10^6 π^+/sec, whereas (π^+, π^-) cross sections are measured with a solid angle of order 10^{-2} sr and incident flux of 5×10^8 π^+/sec. There are significant differences in the signal-to-background. The IAS dominates the forward-angle π^0 spectra at all energies except in a 10-MeV band near 50 MeV. The DIAS is quite difficult to observe in heavy nuclei due to the background on nonanalog state transitions. Attempts to measure DIAS cross sections at 164 MeV on heavy nuclei have failed. At 292 MeV, it was possible, quite recently, to observe the DIAS in ^{208}Pb. Thus, at this energy the data now extend from $A = 14$ to 209. For energies below 100 MeV the data are limited to nuclei with $A \leq 56$.

Representative spectra for (π^+, π^-) reactions are shown for ^{14}C, ^{88}Sr, ^{90}Zr, and ^{208}Pb in Figs. 22 to 24. For ^{14}C, the DIAS cross sections have been measured from 20

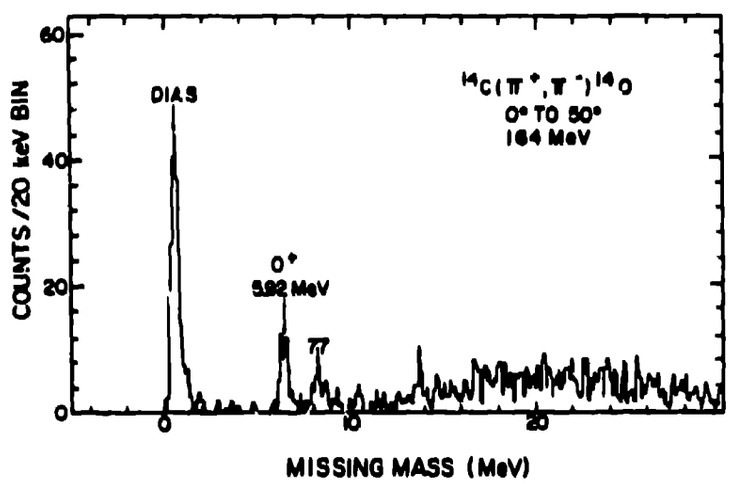

Fig. 22. Measured spectrum[24] for the ^{14}C(π^+, π^-) reaction at 164 MeV.

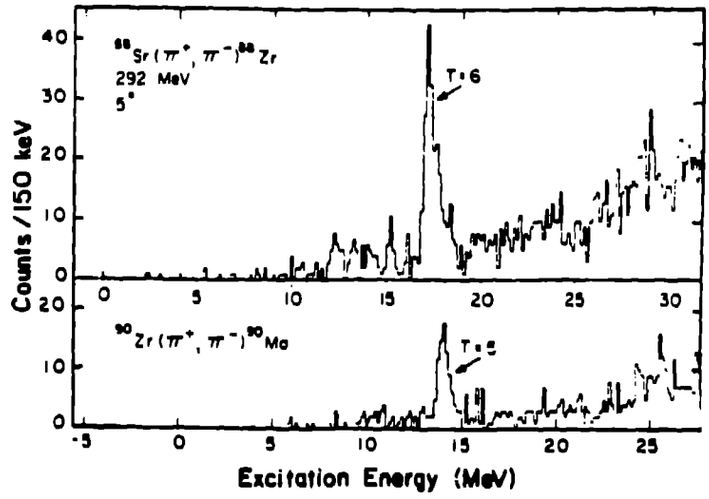

Fig. 23. Spectra for the (π^+, π^-) reaction at 292 MeV and 5° for ^{88}Sr and ^{90}Zr (Ref. 25).

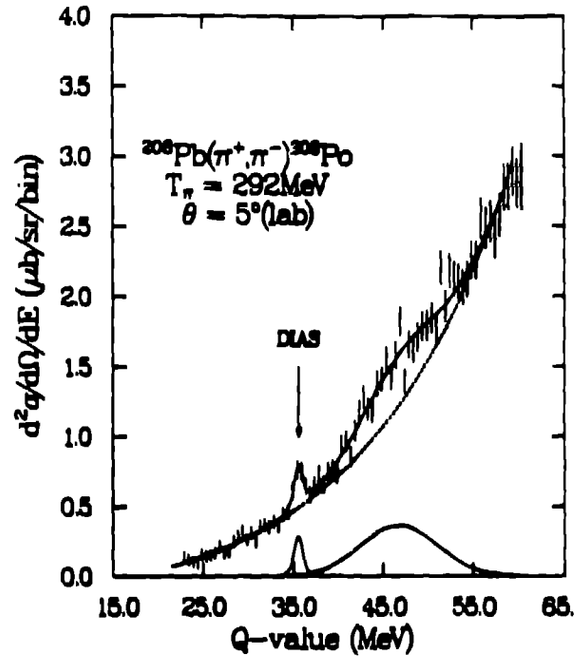

Fig. 24. The measured π^- spectrum of the DCX reaction on ^{208}Pb (Ref. 26). The DIAS is clearly observed and its energy and width have been determined. The solid line plotted with the data represents a 3-component fit assuming a polynomial function background and two Breit-Wigner resonance curves, as shown. Only the DIAS is of interest here.

to 295 MeV, giving a rather complete picture of the behavior of forward-angle cross sections. For the medium-mass nuclei ^{88}Sr and ^{90}Zr, the DIAS is easily observed at 292 MeV, but has been difficult to observe at resonance energies. For heavy nuclei, such as ^{209}Bi and ^{209}Pb, the DIAS is difficult to observe, even at 295 MeV. The spectrum for the ^{208}Pb(π^+, π^-) reaction shown in Fig. 24 took[26] about 3 days running at EPICS. The observation of the DIAS signal is beyond question.

The measurement of the DIAS signal in heavy nuclei makes possible the further study of the isobaric-mass-multiplet equation and of isospin mixing in nuclear states. The measured[26] DIAS excitation energy and width of this state are 32.47 ± 0.17 MeV and 0.85 ± 0.40 MeV (FWHM), respectively. On the assumption that the widths of IAS and DIAS states are due to Coulomb mixing of $T_0 - 1$ background states, one expects Γ (DIAS) $= 2\Gamma$ (IAS). The width of the ^{208}Pb IAS state has the measured value 0.231 ± 0.006 MeV. Twice this value is consistent with the measured DIAS width. These first measurements establish that the (π^+, π^-) reaction can be used to study these narrow states high in the continuum of heavy nuclei. With modest additional effort much more accurate values of Γ (DIAS) could be obtained.

At the low-pion-energy end of the experimental work, we found[27] in the ^{48}Ca(π^+, π^-) measurements that the DIAS could not be observed at 50 MeV due to the large background on nonanalog states, whereas at 35 MeV it stood out quite clearly. Our attempt to measure the DIAS transition on ^{90}Zr at 50 and 35 MeV failed. Thus, it looks like low-energy DIAS measurements in the next few years will be limited to nuclei with $A \lesssim 60$.

B. Systematics of DIAS Cross Sections

The extensive measurements over the past 10 years have determined quite well the shapes of the forward-angle excitation functions. The cross sections for ^{14}C, ^{18}O, ^{26}Mg, and ^{42}Ca are exhibited in Fig. 25. They exhibit a characteristic shape which has a deep minimum near 180 MeV. The cross sections are largest near 50 MeV where they have a value of about 4 μb/sr.

The 5° cross sections vs A at 292 MeV are shown in Fig. 26. The dashed line, representing the function

$$\frac{d\sigma}{d\Omega}_{\mathrm{DIAS}}(5^\circ) = 19(N - Z)(N - Z - 1)A^{-10/3} \text{ mb/sr}$$

reproduces the data trends and gives the characteristic shape of forward-angle DIAS cross section. The largest cross sections are obtained for the light nuclei, and the smallest for medium-mass nuclei near $A = 50$. For $A \gtrsim 70$, a nearly constant value of 0.8 μb/sr

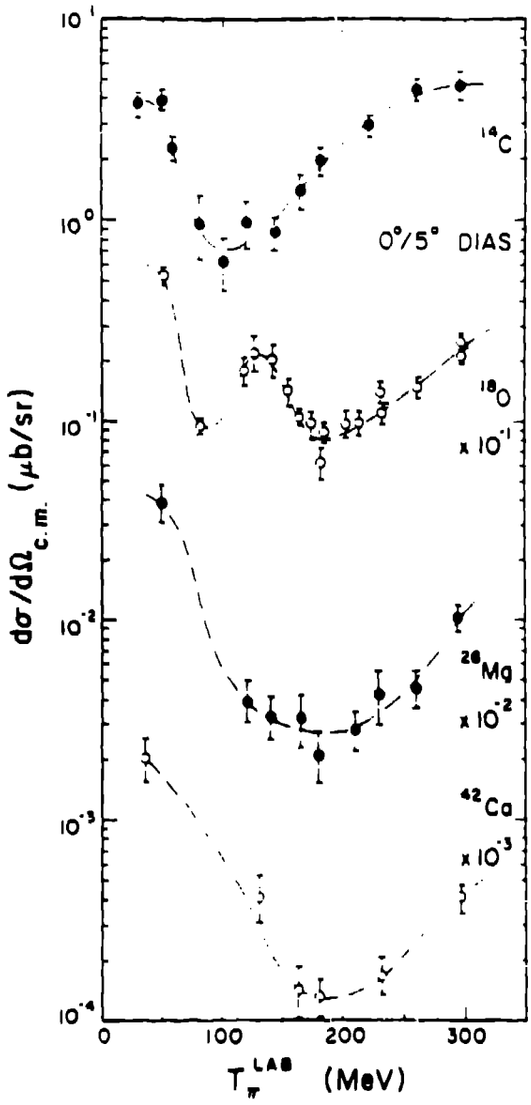

Fig. 25. Forward-angle DIAS cross sections for $T = 1$ nuclei. Data are taken from Refs. 28 through 33. The lines are drawn to guide the eye.

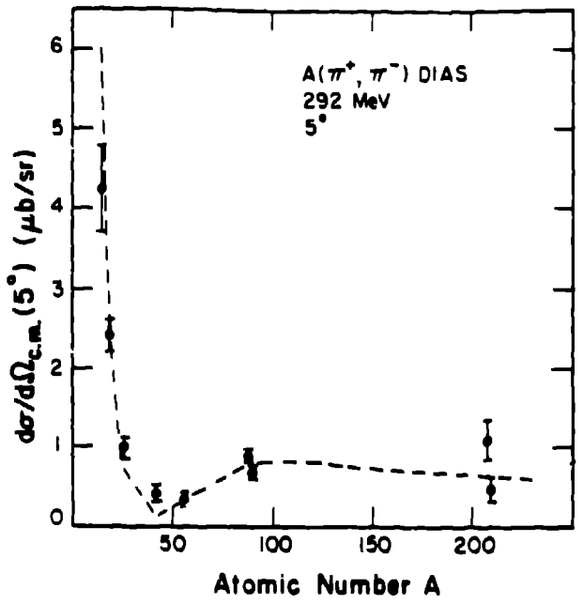

Fig. 26. The A-dependence of the 0° DIAS cross sections[33] at 292 MeV. The dashed line represents the function $19(N-Z)(N-Z-1)A^{-10/3}$ mb/sr.

is obtained. This functional form[18,19] follows from the simplest assumptions about DIAS transitions, viz., that only the valence nucleons are involved, that the intermediate state is the IAS, and that the reaction occurs on the outer limb of the nucleus. The constancy of the DIAS cross section for $A > 70$ results from the fact that for stable heavy nuclei $(N-Z) \sim A^{5/3}$.

The 5° cross sections divided by $(N-Z)(N-Z-1)$ are plotted against A on logarithmic scales in Fig. 27. At 292 MeV all the data points except ^{42}Ca fall closely to the line given by $A^{-10/3}$. At lower energies the data do not cluster so nicely along the $A^{-10/3}$ line, although this power law still describes the general trends. In a recent analysis of all available 5° data between 100 and 300 MeV, Gilman *et al.*[34] found that a fit of A^α to the data at each energy yields a value of α quite close to $-10/3$. Their results are shown in

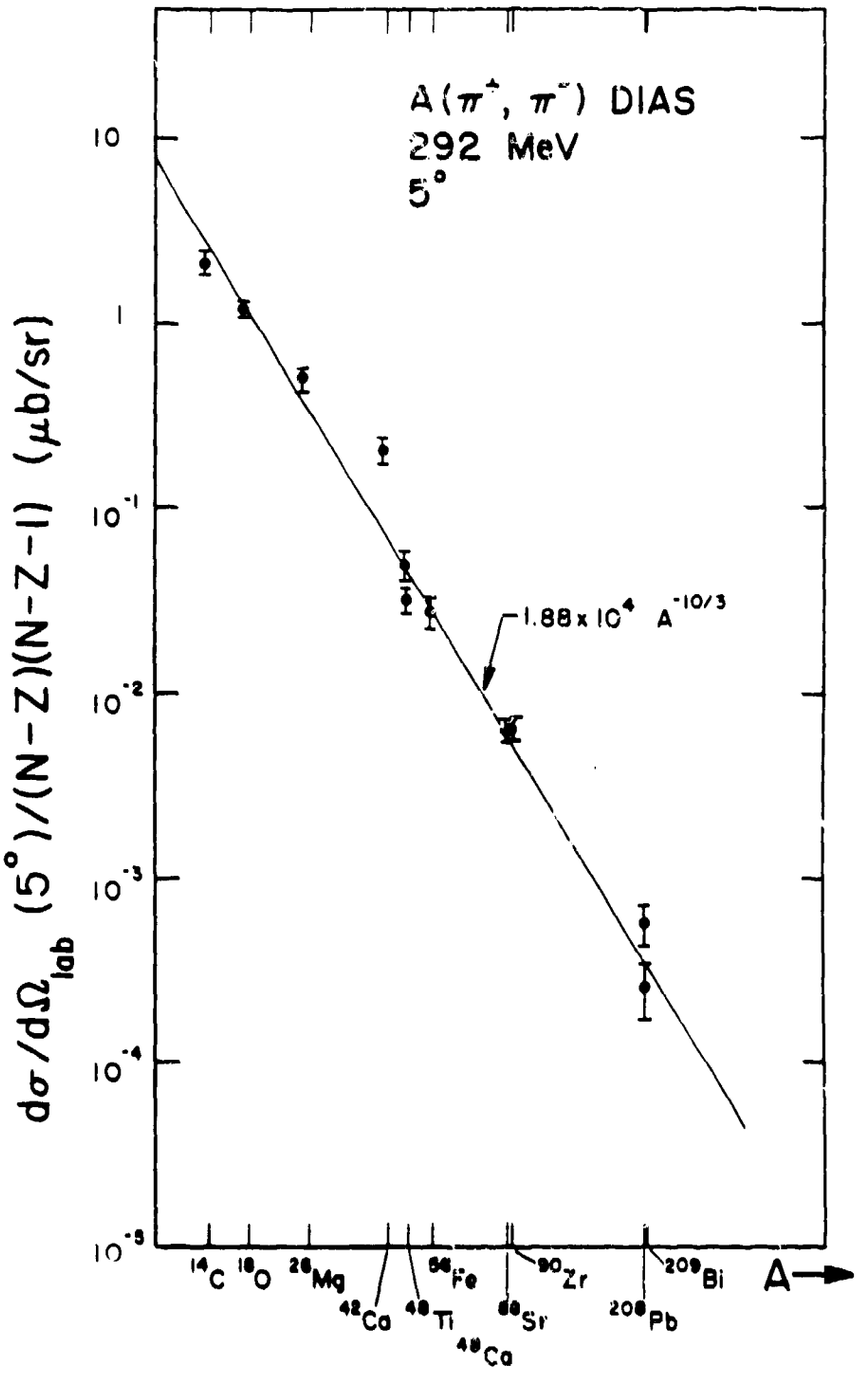

Fig. 27. The A-dependence of 5° DIAS cross sections[33] at 292 MeV. The straight line is a fit to the data assuming an A dependence of $A^{-10/3}$ as expected for the strong absorption model.

Fig. 28. This global trend reflects the surface nature of the reaction over this energy range.

The angular distribution shapes have been quite revealing. At 292 MeV the shapes measured for ^{14}C, ^{18}O, and ^{26}Mg were found[24] to have first minima at the expected position for simple diffraction scattering. However, at 164 MeV, the angular distributions have first minima at angles smaller than expected from a simple diffraction picture.[24] An interference of two amplitudes would seem to be required to explain these data. Theoretical efforts to understand these angular distribution shapes have pointed to a significant role of short-range phenomena in one of the amplitudes. We discuss such an analysis next.

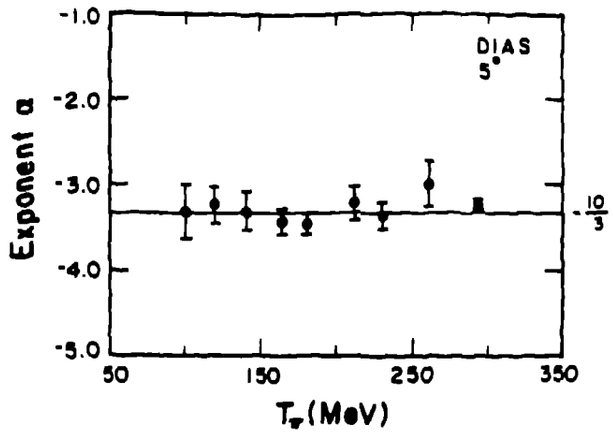

Fig. 28. Values of α determined by Gilman *et al.*[34] in fits of the functions $(N-Z)(N-Z-1)A^{\alpha}$ to 5° DIAS cross sections.

C. Optical Potential Analyses

The puzzling angular distribution shapes at 164 MeV prompted Johnson and Siciliano[35] to investigate the role of higher-order terms in the π-A optical potential. To achieve a unified analysis of elastic scattering, IAS transitions, and DIAS transitions, they cast the optical potential in a form that explicitly incorporates isospin invariance. The general form they employed is

$$U = U_0 + U_1(\vec{t}_\pi \cdot \vec{T}_A) + U_2(\vec{t}_\pi \cdot \vec{T}_A)^2 \quad .$$

Here $\vec{t}_\pi$ is the isospin of the pion and $\vec{T}_A$ is the isospin of the nuclear target. U_0, U_1, and U_2 are referred to as the isoscalar, isovector, and isotensor components of the optical potential. The separation of the optical potential into these three terms has the advantage that each term is particularly sensitive to one of the scattering processes: U_0 is determined primarily by elastic scattering; U_1 is most directly sensitive to IAS cross sections; and U_2 is most directly sensitive to DIAS cross sections. Dynamical processes associated with each term for scattering near resonance energies are illustrated in Fig. 29. With this form of the potential there are two amplitudes for the DIAS. One, obtained by the iterated operation of the U_1 term, goes through the IAS. The other, given by U_2, gives transitions through other intermediate states or through new short-range mechanisms. One type of interaction

term that contributes to U_2 is the Δ-N interaction (DINT) term such as is illustrated in Fig. 29.

In the model of Johnson and Siciliano, U_0, U_1, and U_2 are expressed as series expansions in ρ and $\Delta\rho$, where $\rho = \rho_n + \rho_p$ and $\Delta\rho = \rho_n - \rho_p$. In a first-order calculation only ρ and $\Delta\rho$ terms are retained for U_0 and U_1; U_2 is dropped, since its lowest-order terms are quadratic in $\Delta\rho$. In second-order calculations, terms ρ^2, $\rho\Delta\rho$, and $\Delta\rho^2$ are retained in U_0, U_1, and U_2.

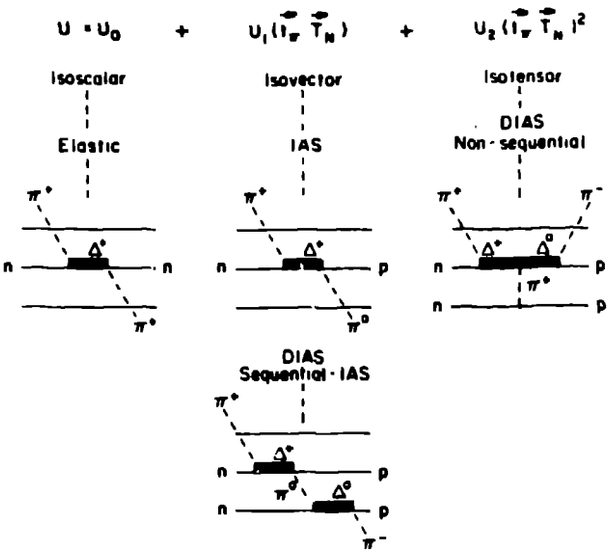

Fig. 29. The form of the π-A optical potential as used in the analysis of Johnson and Siciliano.[35] The IAS transition is induced by the U_1 term. The DIAS transition is induced by sequential operation of U_1 and by the U_2 term. The latter allows for transitions through nonanalog intermediate states.

First Order. At this level, DIAS transitions are calculated as sequential single-charge-exchange scattering through the IAS intermediate state. Such calculations, with some parameter adjustments, account for many of the general features of IAS and DIAS transitions, such as the trends of 0° cross sections with $(N - Z)$ and A, and the general shapes of elastic and IAS angular distributions at forward angles. The most notable failures of the first-order calculations occurs in the absolute magnitudes of IAS and DIAS cross sections and the shapes of DIAS angular distributions. On a fundamental level, first-order calculations are known to leave out important dynamical effects associated with pion absorption, Δ propagation, N-Δ interactions, and N-N correlations.

Second-Order Unified Analysis. Using an optical potential of the form given above, Greene *et al.*[36] performed a unified analysis of 164-MeV data for elastic, IAS, and DIAS scattering. This gave an excellent quantitative description of elastic scattering for nuclei from ^{12}C to ^{40}Ca, forward-angle IAS cross sections for nuclei from ^{7}Li to ^{208}Pb, and DIAS cross sections at 5° for nuclei from ^{14}C to ^{50}Fe. The theoretical DIAS cross sections are compared with the data in Fig. 30. In addition, the DIAS angular distributions between 0 and 60° for ^{14}C, ^{18}O, and ^{26}Mg were quite well described, as is shown in Fig. 31. The last result could be obtained only with the inclusion of a large U_2 term. Since this term can

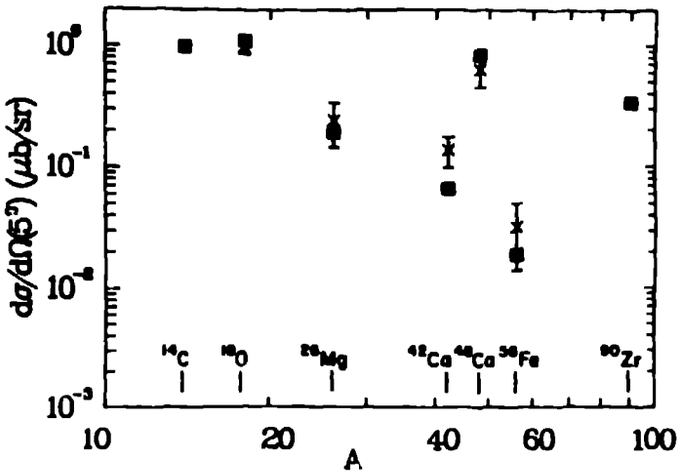

Fig. 30. Comparison of experimental 5° DIAS cross sections with the second-order optical potential calculation of Greene *et al.*[36] (shown as solid squares).

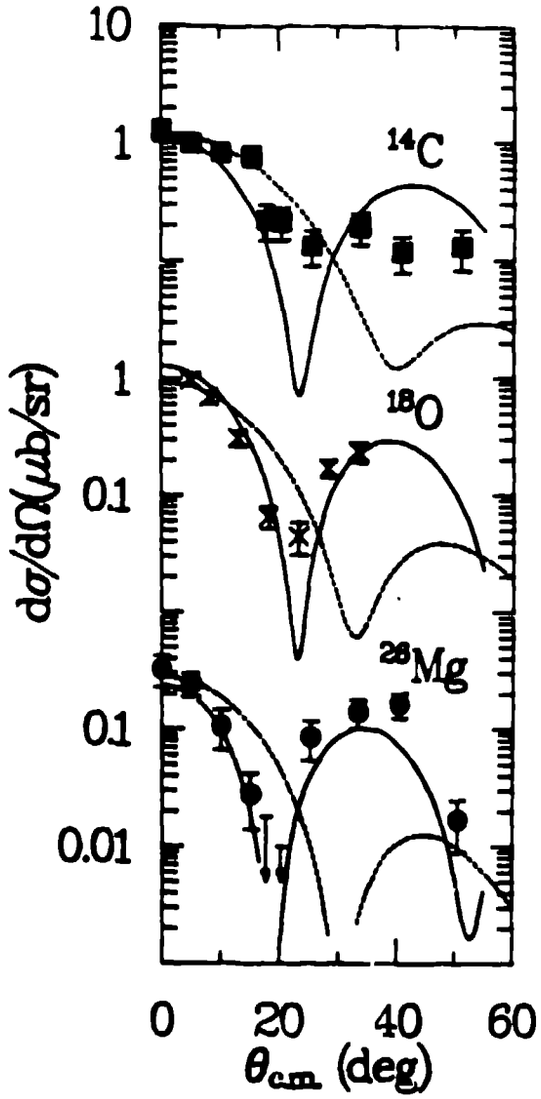

Fig. 31. First-order (dotted line) and second-order (solid line) optical potential calculations of Greene *et al.*[36] for the DIAS transitions at 164 MeV on ^{14}C, ^{18}O and ^{26}Mg.

have its origin in Δ-N interaction terms such as the one shown in Fig. 29, Greene *et al.* concluded that DIAS transitions at 164 MeV are quite sensitive to short-range correlations.

We see that availability of extensive IAS and DIAS data at resonance energies, together with a theoretical model incorporating isospin invariance, gives a quantitative basis for investigating the short-range dynamics involved.

IV. USING DCX AT LOW PION ENERGIES TO STUDY N-N CORRELATIONS

A. The ^{14}C Puzzle

If one examines the forward-angle spectra of the $^{14}C(\pi^+, \pi^0)$ reaction as a function of incident beam energy between 20 and 100 MeV, one feature stands out. This can be seen

in Fig. 32. The IAS completely disappears at 50 MeV, whereas it stands out prominently at other energies. The measured 0° cross sections as a function of energy are shown in Fig. 20. In view of the small IAS cross sections at 50 MeV, it came as a surprise when Miller[37] predicted a large 0° cross section of 12 μb/sr for the DIAS transition at 50 MeV. At higher energies the DIAS cross sections are typically $\lesssim 1$ μb/sr.

Miller's prediction was based on a hybrid quark-nucleon model designed to deal with short-range N-N components found in ordinary nuclear wave functions. In this model, two nucleons lose their separate identities when they come close together, forming a six-quark cluster. The probability for this is governed by r_0, the two-nucleon separation distance. Miller used the value $r_0 = 0.95$ fm, which gives a six-quark cluster probability of 6% for ^{14}C. To calculate the scattering amplitude the pions are coupled directly to the quarks inside the bag via an axial-vector operator of the form

$$g_{\pi N}\vec{\sigma}_j \cdot \vec{k}_\pi \tau_+$$

where $\vec{\sigma}_j$ is the quark spin operator, k_π is the pion momentum, τ_+ is the charge-changing operator, changing a down quark to an up quark, and $g_{\pi N}$ is the experimentally determined pion-nucleon coupling constant.

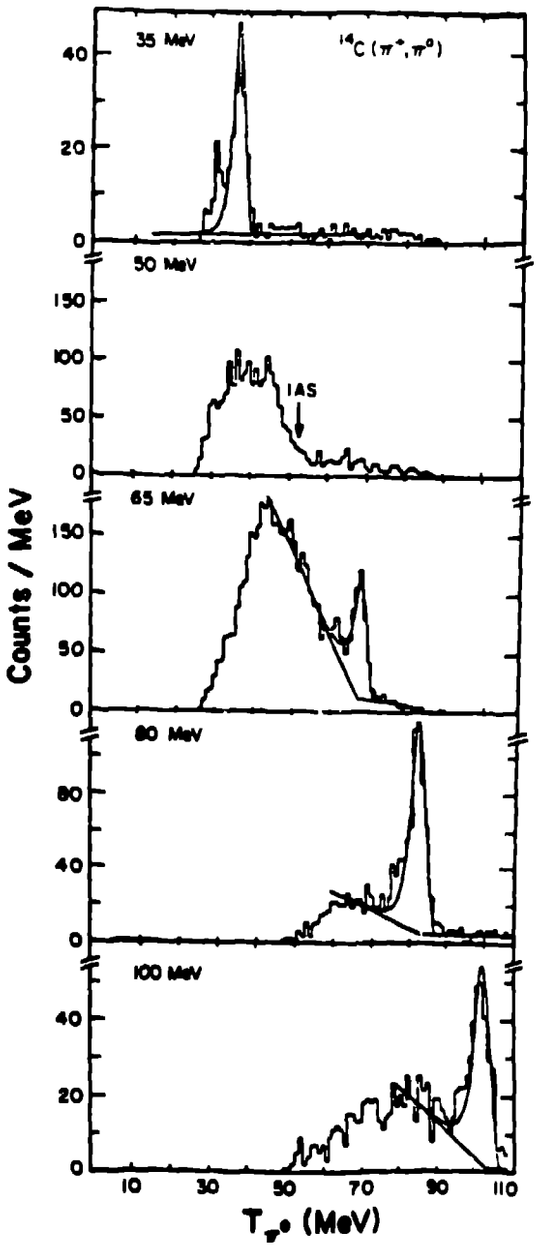

Fig. 32. Spectra for the ^{14}C(π^+,π^0) reaction measured[21] at forward angles (0 to 10°) at different energies. The IAS is seen to disappear at 50 MeV.

The results of Miller's predictions[37] are compared with the LAMPF data[28] in Fig. 33. The pronounced forward peak is certainly seen in the data, although the measured 0° cross section of 3.9 ± 0.4 μb/sr is less than predicted. Miller subsequently[38] corrected his original plane-wave calculation by including a pion absorption factor of $\exp(\ell/\lambda)$, which lowered the 0° cross section to 4 μb/sr.

Optical potential calculations based on sequential scattering through the analog intermediate state considerably underestimate the forward-angle cross section. A representative calculation is shown in Fig. 33.

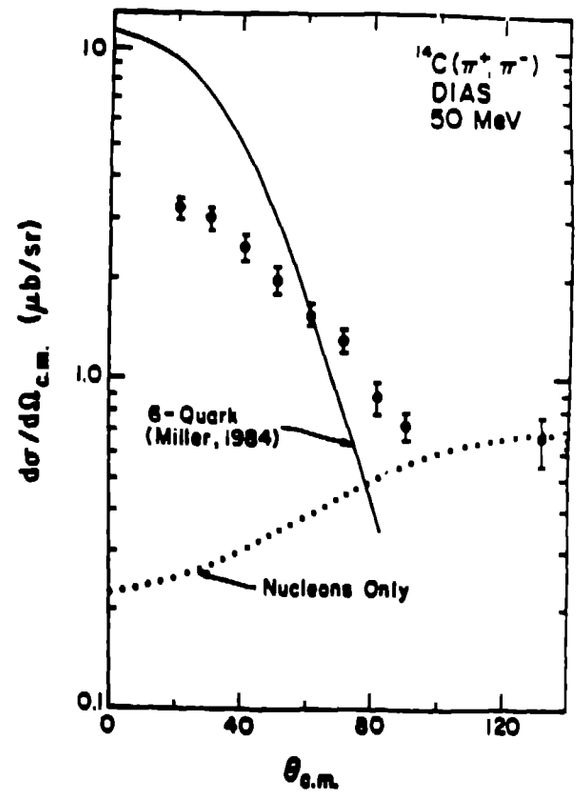

Fig. 33. Differential cross sections for the DIAS transition on ^{14}C. The data and the dotted curve are from Ref. 28. The solid curve is from Ref. 37.

This situation prompted Gibbs, Kaufmann, and Siegel[39] to calculate both IAS and DIAS cross sections for ^{14}C using their multiple scattering theory. With their model they could give detailed information on the range and angles involved for the intermediate pion propagation. They gave a geometrical answer as to how SCX could be small at 0° and DCX could be large. It was two 90° SCX scatterings that gave a large 0° DIAS cross section. The distance traveled by the intermediate π^0 was also calculated, and they obtained the result that approximately 50% of the scattering amplitude arose from scatterings where the two nucleons were within 1 fm of each other. Thus, their calculations lent support to Miller's contention that large DIAS cross sections at 0° signified a large role of short-range N-N components.

Higher-order optical potential treatments by Siciliano *et al.*[40,41] and Liu[42] were also able to reproduce the IAS and DIAS cross sections. The higher-order terms are thought to represent short-range effects.

A different conclusion was reached by Karapiperis and Kobayashi,[43] who used the Δ-hole model to calculate the IAS and DIAS cross sections for ^{14}C. They claimed that

the DIAS transition does not involve appreciable contributions from short-range N-N correlations.

Considerable effort has gone into resolving this question. We will review these results. They suggest a tentative answer to the above question.

B. DCX Mechanisms

The classification of DCX mechanisms is less than straightforward because different theoretical formulations are used to describe the same phenomena. There are at least six distinct approaches:

1. Optical potential phenomenology (e.g., Refs. 35, 41, 42, and 44).
2. Multiple scattering treatments (e.g., Ref. 39).
3. Glauber model (e.g., Ref. 46).
4. Δ-hole model (e.g., Refs. 43 and 48).
5. Meson exchange currents (e.g., Ref. 47).
6. Six-quark bags (e.g., Refs. 37 and 49).

Since we are interested in determining what the range of double scattering is, and particularly we would like to see if the short-range N-N dynamics of DCX reactions can be isolated, the problem is to determine whether the various approaches reach the same answer on this point.

A basic distinction in the approaches is whether they assume *sequential scattering* or some *specialized short-range DCX mechanism.* By sequential scattering, we mean that the π^+ of the beam charge exchanges on a neutron to produce a π^0, which propagates to another neutron where it charge exchanges to produce a π^-, which then leaves the nucleus and is detected. This process can be broken into two contributions, depending on whether the intermediate nuclear state is the IAS or whether it is a set of other states. This picture for sequential scattering is illustrated in Fig. 34.

Some explicitly short-range DCX mechanisms are illustrated in Fig. 35. These give a quite different picture of DCX. In the six-quark bag picture, two neutrons momentarily form a six-quark bag. While in this condition, a π^+ is absorbed and a π^- is emitted, converting two down quarks to two up quarks. In the Δ-interaction (DINT) diagram a neutron accepts the π^+ and later, after brushing off a π^+, radiates a π^-. This resembles elastic scattering on a single nucleon. In the meson exchange process, the π^+ beam double-charge exchanges on a virtual pion in transit between two nucleons. All three of these processes are manifestly short-range processes.

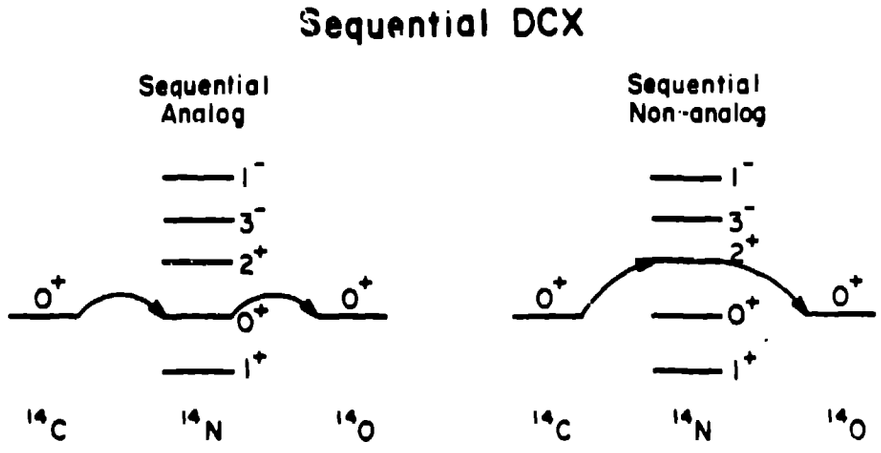

Fig. 34. Illustration of the two types of sequential scattering involved in DIAS transitions.

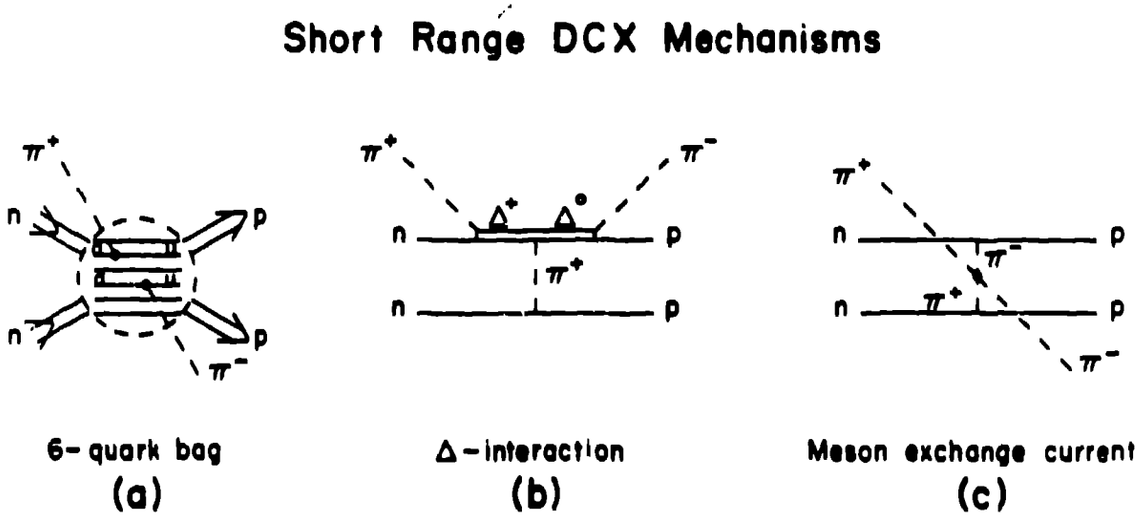

Fig. 35. Illustration of short-range DCX mechanisms discussed in the text.

The sequential scattering processes discussed above may also contain short-range components. In fact, we have already noted that the sequential scattering calculations of Gibbs *et al.*[39] explicitly show short-range components. Fruitful investigations of sequential scattering have occurred in the past year, and we now turn to a discussion of these results.

C. Sequential Scattering Treatments

Bleszynski and Glauber[50] have just completed a detailed analysis of the IAS and DIAS transitions in ^{14}C using a sequential scattering picture. Their study is particularly instructive regarding the role played by the spatial correlations in the valence nucleons. As a general result, they find that the correlations contained within proven shell model wave functions are adequate to give a satisfactory account of both the IAS and DIAS transitions at 50 MeV. Their calculations are compared with the data in Fig. 36. For these calculations the Cohen and Kurath wave functions[51] for the ^{14}C ground state were employed. The role of distortions was found to be minimal. The two sets of curves represent plane-wave impulse approximation calculations and distorted-wave impulse approximation calculations.

The Cohen-Kurath wave functions evidently contain the correct spatial correlations. In an LS coupling scheme, as used in Ref. 50, there are only two components in the ^{14}C wave function,

$$| \, ^{14}C, \text{ g.s.}\rangle = \alpha \, | \, ^1S_0\rangle + \beta \, | \, ^3P_0\rangle \quad ,$$

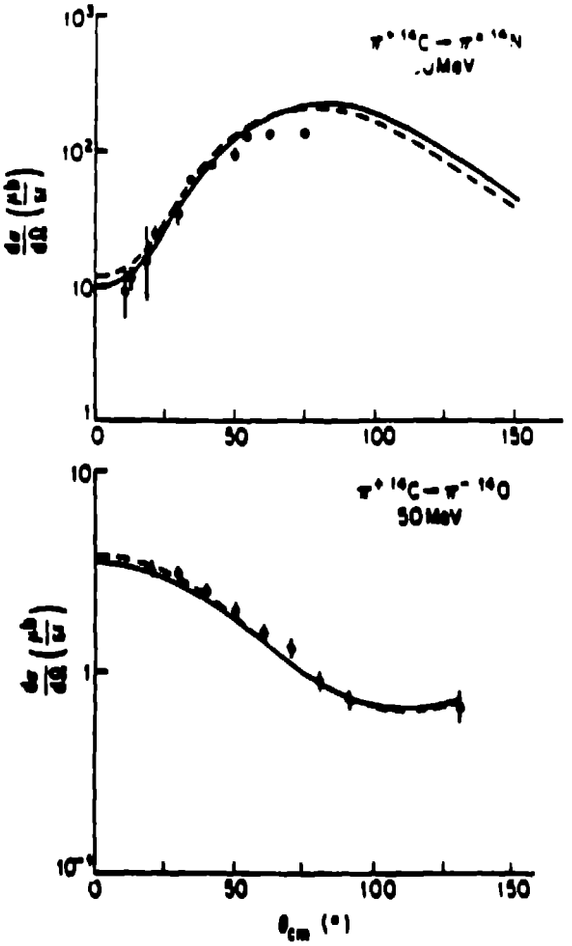

Fig. 36. Comparison of the calculations of Bleszynski and Glauber[50] with the ^{14}C data on the IAS and DIAS transitions (Refs. 21 and 28). The dashed and solid curves correspond to plane-wave and distorted-wave calculations, respectively.

assuming that only p-shell nucleons are active. The calculations shown in Fig. 36 used values $|\alpha| = 0.85$ and $|\beta| = 0.52$ corresponding to the Cohen-Kurath values. The DIAS angular distribution would have looked quite different for $\alpha = 1$ or for $\beta = 1$ as is shown in Fig. 37. The forward peaking of the angular distribution is due to the $^1S_0$ component. In this state of relative motion the nucleons can move on top of each other ($\vec{r}_1 \approx \vec{r}_2$), whereas in the $^3P_0$ state, which is spatially antisymmetric, the wave function vanishes

for $\vec{r}_1 = \vec{r}_2$. Thus, pronounced forward peaking is seen to be a signature of short-range spatial correlations.

Bleszynski and Glauber investigated this point more quantitatively by expressing the double-scattering amplitude in terms of the relative coordinate $\vec{r} = \vec{r}_1 - \vec{r}_2$ and centroid coordinate $\vec{R} = \frac{1}{2}(\vec{r}_1 + \vec{r}_2)$. The factor which contains the dependence on the relative coordinate is $\Omega(\vec{r}, \vec{R}, \Lambda)$. The averaged and weighted value of this function, so as to reflect appropriately the dependence on internucleon distance r, is displayed in Fig. 38. This curve shows that most of the DCX occurs at distances smaller than 2 fm and that the most probable distance of separation is 1.2 fm. These results are quite consistent with the earlier results of Gibbs *et al.*[39] In view of the fact that the rms charge radius of the proton is 0.7 fm, one would have to conclude that there is considerable overlap of the two nucleons as they are converted from neutrons to protons.

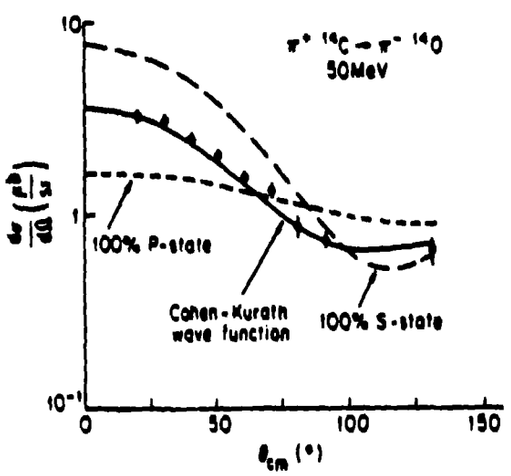

Fig. 37. Comparison of the ^{14}C data with calculations[50] using different model wave functions, as discussed in the text.

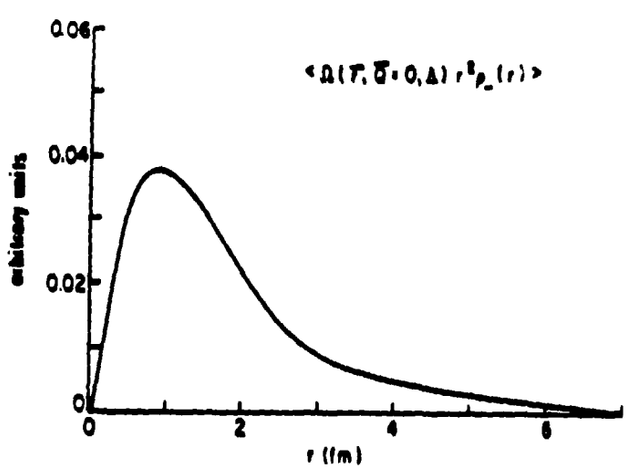

Fig. 38. The function $|\,\Omega(\vec{r}, \vec{Q} = 0; \Lambda)\,|$ $r^2\rho(r)$ as defined in Ref. 50, with $\Lambda = 3.5\ \mathrm{fm}^{-1}$, and averaged over orientations of $\vec{r}$ (see text).

A further result given by Bleszynski and Glauber is an evaluation of the role of the IAS intermediate state. For the full DIAS amplitude, they summed over all accessible intermediate states (closure). When only the IAS intermediate state is included, they obtain a flat angular distribution, as is shown in Fig. 39. They point out that restricting the intermediate state to the IAS corresponds to omitting N-N correlations.

The large role of nonanalog intermediate states at 50 MeV for the ^{14}C DIAS transitions was noted earlier in Refs. 39 and 43. Calculations with optical potentials[41,42] also point to a large role of nonanalog intermediate states.

Thus, three points emerge from analyses of the ^{14}C data: (1) forward-angle DIAS cross sections at 50 MeV arise predominantly from scatterings through nonanalog intermediate states; (2) N-N correlations are responsible for the transitions through the nonanalog intermediate states; and (3) most DIAS transition strength involves nucleon correlations with $r < 2$ fm.

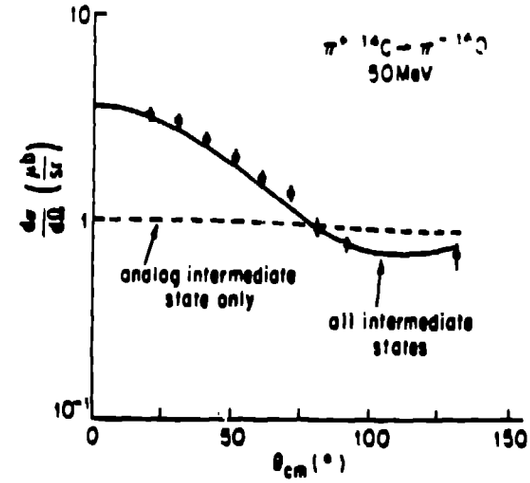

Fig. 39. Comparison of the ^{14}C DIAS data with calculations of Ref. 50. The dashed curve results when only the IAS intermediate state is included; the solid curve results from a sum over all intermediate states.

D. DIAS Transitions on $^{42,44,48}Ca$

The Ca isotopes offer an attractive opportunity to study further the effects of nucleon correlations. To this end we measured[27,29] the isotopes Ca-42,44,48, which have 2, 4, and 8 valence neutrons in the $1f_{7/2}$ shell, respectively. Our initial, naive expectation, before we fully appreciated the large role played by N-N correlations, was that the cross sections would increase with the addition of valence neutrons. This was based on the apparent success of the low-energy plane-wave model of Koltun and Reitan,[52] which predicts a $(N-Z)(N-Z-1)$ dependence and a very weak A-dependence. This model explained the near-constancy of the measured 50-MeV cross sections for the $T = 1$ nuclei ^{14}C, ^{18}O, and ^{26}Mg. In our first run on ^{48}Ca we were quite surprised to learn that the ^{48}Ca cross section has about the same value as that of ^{14}C. Since the factor $(N-Z)(N-Z-1)$ is 28 times larger for ^{48}Ca than for ^{14}C, this result was quite puzzling. It looked like a significant A-dependence had developed at $A > 26$. In our second run we measured $^{42,44}Ca$ and found ^{44}Ca to have about one-half the cross section of ^{42}Ca. The spectra are shown in Fig. 40 and the cross sections are given in Table II. This result showed convincingly that A-dependence was not the dominant effect. It was highly suggestive of an interference effect having its origin in shell-model correlations.

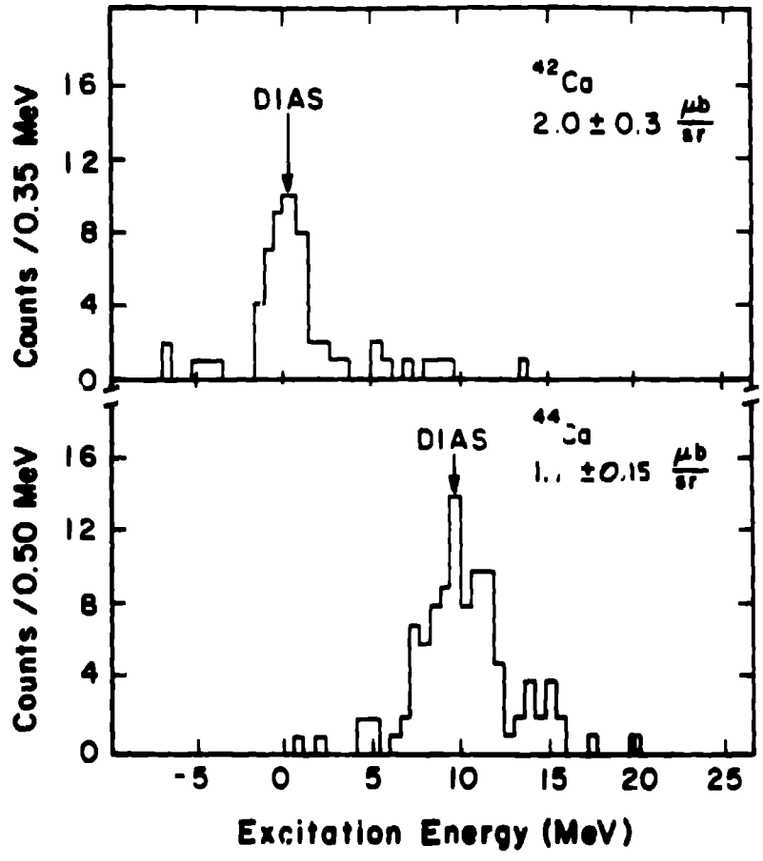

Fig. 40. Measured spectra[27,29] for the ^{42,44}Ca(π^+, π^-) reactions at 35 MeV and 40°.

Table II. The measured laboratory cross sections for the calcium isotopes at a laboratory scattering angle of 40° (Refs. 27 and 29).

Isotope	T_π[a] *(MeV)*	$d\sigma/d\Omega$ *(μb/sr)*	*Relative Uncertainties*[b] *(μb/sr)*
^{42}Ca	33.6	2.0 ± 0.5	(±0.3)
^{44}Ca	32.0	1.1 ± 0.3	(±0.15)
^{48}Ca	34.2	2.4 ± 0.7	(±0.6)

[a]Kinetic energy at the center of the target.
[b]Relative uncertainties appropriate for the isotopic comparison.

By this time E. Bleszynski, M. Bleszynski, and Glauber had begun calculations which showed that there were large differences in the two-body correlation densities in $(f_{7/2})^n$ configurations for different values of n. A comparison of ^{42}Ca and ^{48}Ca is shown in Fig. 41 (Ref. 53). What is plotted is the "separation density" which is defined by

$$\rho_{sep}(\vec{r}) = \int d^3R\rho^{(2)}(\vec{R}+\vec{r}/2,\vec{R}-\vec{r}/2)$$

with

$$\rho^{(2)}(\vec{r}_1,\vec{r}_2) = \rho^{(1)}(\vec{r}_1)\rho^{(1)}(\vec{r}_2)[1+C(\vec{r}_1,\vec{r}_2)] \ .$$

In these expressions $\rho^{(2)}(\vec{r}_1,\vec{r}_2)$ is the two-particle density, $\rho^{(1)}(\vec{r})$ is the single-particle density, and $C(\vec{r}_1,\vec{r}_2)$ is the shell-model correlation function. To omit N-N correlations corresponds to setting $C = 0$.

For the two valence nucleons of ^{42}Ca (as well as ^{14}C), there is a large amount of spatial overlap in the two-particle wave function, giving an increased value of ρ_{sep} for small r (Fig. 41). For ^{48}Ca, which has eight valence neutrons in a closed $f_{7/2}$ shell, the Pauli exclusion principle enormously reduces ρ_{sep} at small r. For ^{44}Ca, $\rho_{sep}(r)$ is intermediate to ^{42}Ca and ^{48}Ca. If indeed the DIAS transitions are most sensitive to the small r behavior of $\rho_{sep}(r)$, one can see a qualitative explanation for the behavior of the ^{42,44,48}Ca cross sections. We discuss this below. Full calculations of the Ca cross sections taking into account the shell model correlations and the π-N interaction are now in progress.[53,54]

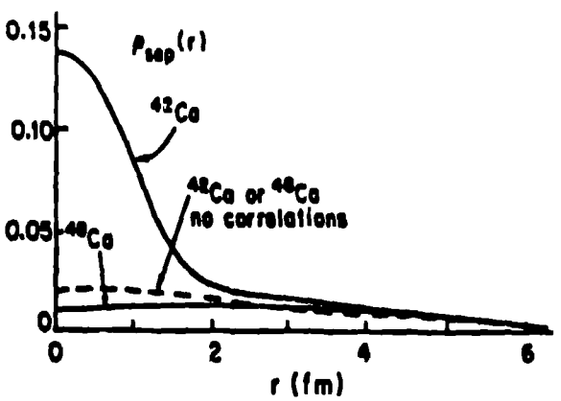

Fig. 41. Separation densities for $(f_{7/2})^n$ configurations as given in Ref. 53.

E. Two-Amplitude Shell Model

A useful formulation of the DIAS scattering amplitude in terms of analog and nonanalog components was given recently by Auerbach, Gibbs, and Piasetzky.[55] If there are n neutrons in shell j and they are all coupled pairwise to $J = 0$ (seniority = 0 configuration), the (π^+,π^-) DIAS cross section can be written as

$$\frac{d\sigma}{d\Omega}_{\rm DIAS}(\theta) = \frac{(N-Z)(N-Z-1)}{2}|A(\theta)+\omega B(\theta)|^2$$

where the amplitude A represents the $L = 0$ multipolarity of the two-body transition operator and the amplitude B represents a sum over all $L \neq 0$ even multipoles. The weighting factor ω for the B amplitude depends on N and Z according to

$$\omega = \frac{(2j + 3 - 2n)}{(n-1)(2j-1)} ,$$

where $n = N - Z$. We note that ω has values 1, 1/9, -1/7 for Ca-42,44,48, respectively. We see that if $| B | \gtrsim | A |$ there can be dramatic deviations from $(N - Z)(N - Z - 1)$ scaling across the Ca isotopes.

Since the A amplitude represents the $L = 0$ transition multipole, it represents predominantly the IAS intermediate state. (There may be small $L = 0$ components in nonanalog states.) The B-term represents the sum over all nonanalog intermediate states. As we saw from the ^{14}C analyses, there is considerable evidence that the forward-angle DIAS cross sections at 50 MeV derive most of their strength from nonanalog intermediate states. Thus we might expect $| B |>| A |$.

The data on the three Ca isotopes allow us to determine empirically $| A |$, $| B |$, and the relative phase between A and B. The values determined from the data are given in Table III. The value $| B | / | A | = 3.5$ is obtained. This implies that for ^{42}Ca, where $\omega = 1$, the DIAS amplitude at 40° arises primarily from nonanalog intermediate states. For ^{44}Ca and ^{48}Ca the DIAS amplitudes arise predominantly from the IAS intermediate state, since the weighting factors of 1/9 and $-1/7$ greatly suppress the nonanalog amplitude. In terms of the N-N correlations, we have seen from the calculations of Ref. 53 that $\rho_{sep}(r)$ for ^{42}Ca is large at small r and relatively flat for ^{44,48}Ca. Thus, the Ca cross sections at low energy are quite naturally explained as a consequence of the N-N correlations in $(1f_{7/2})^n$ wave functions and the short-range nature of the double-scattering process.

Table III. The deduced magnitudes of A, B, and ϕ (relative phase angle) from the data in Table II. The units for A and B are $(\mu b)^{1/2}$.

$\| A \|$	$\| B \|$	ϕ	$\| B \| / \| A \|$
0.34	1.45	59°	3.5

Preliminary results from Kaufmann and Gibbs[55] indicate that the largest values of $|B|/|A|$ at forward angles occur near 50 MeV. Values of this ratio at 0° as a function of beam energy for the DIAS transition in $(f_{7/2})^n$ configurations are shown in Fig. 42. There is a pronounced peak near 50 MeV. By maximizing the $|B/A|$ ratio one gains maximum sensitivity to short-range N-N correlations. This is shown explicitly in Fig. 43, which shows the internucleon range r involved for both the A and B amplitudes. It is seen that A is relatively flat with r, whereas B is sharply peaked at small r.

From these results, we would conclude that measuring 0° DIAS cross sections near 50 MeV is an optimum way to study short-range nucleon correlations.

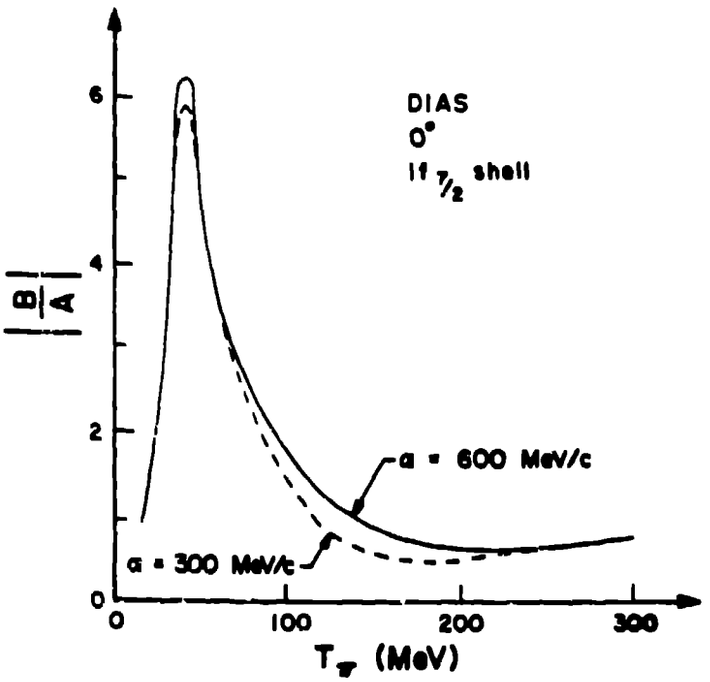

Fig. 42. Theoretical values[54] of the ratios of the two-body transition amplitudes $|A|$ and $|B|$ as defined in the text. These were calculated using the theoretical formulation of Ref. 39.

V. SUMMARY AND CONCLUSIONS

We have followed in this article the progress in the measurement and analysis of the IAS and DIAS transitions of pion-charge exchange reactions. I believe we have the following results.

(1) <u>*IAS transitions:*</u> The measurements now determine quite well the patterns of the forward-angle cross sections in the energy range 20 to 500 MeV for nuclei from ^{1}H to ^{208}Pb. Empirical relations have been found to systematize the resonance energy data. These serve to characterize the isovector part of the π-A optical potential. Between 300 and 425 MeV the IAS cross sections increase by factors of 2 to 3, a feature which has not yet been fully incorporated into theoretical treatments. Qualitatively, this increase reflects a greater volume scattering at high pion energies. At low pion energies the forward-angle IAS cross sections exhibit a deep minimum near 50 MeV, a feature originating in the free $\pi^- p \rightarrow \pi^0 n$ cross sections. Its persistence in π-A scattering places strong constraints on dispersive medium effects.

(2) *DIAS transitions:* There now exists an extensive body of data at energies 20 to 300 MeV which establishes the systematics of forward-angle cross sections. Interest in these data continues to center on the unambiguous identification of the role of short-range N-N correlations and on the magnitude of the Δ-N interaction term. At resonance energies the anomalous angular distribution shapes appear to signify short-range effects. At low pion energies, the observed forward-peaked angular distributions seem to be signatures of short-range effects. The anomalous cross section ratios for ^{42,44,48}Ca can be understood as being a consequence of the short-range nature of the DCX process, and indeed give strong support to such a conclusion.

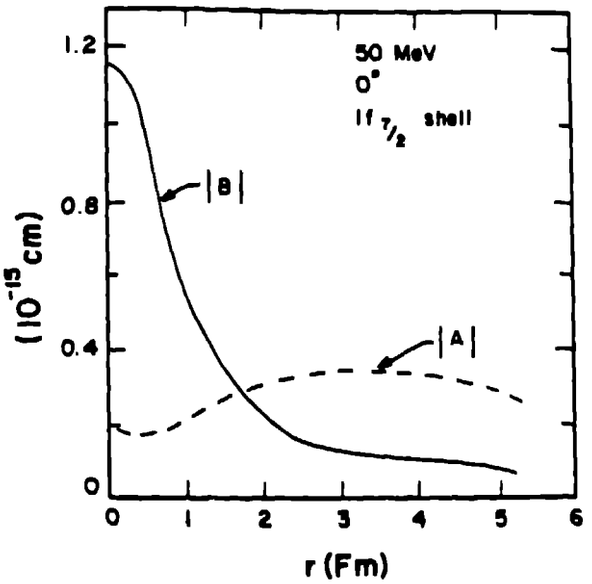

Fig. 43. Theoretical values[54] of $|A|$ and $|B|$ (defined in the text) as a function of cutoff radius r.

Although quark degrees of freedom have been employed to describe short-range features of DCX reactions, to date there is no unique signature to the role of quarks. One can hope that as more conventional analyses provide an unambiguous identification of the short-range components in DCX reactions, the role of quark degrees of freedom may be seen.

REFERENCES

1. F. Ajzenberg-Selove, *Nuclear Physics* **A360**, 56 (1981).
2. D. B Holtkamp, S. J. Seestrom-Morris, D. Dehnhard, H. W. Baer, C. L. Morris, S. J. Greene, C. J. Harvey, D. Kurath, J. A. Carr, *Physical Review C* **31**, 957 (1985).
3. W. J. Courtney and J. D. Fox, *Atomic Data and Nuclear Data Tables* **15**, 141 (1975).
4. E. R. Siciliano, private communication; based on methods of Ref. 5.
5. J. W. Negele and D. Vautherin, *Physical Review C* **5**, 1472 (1972); M. Beiner, H. Flocard, N. Van Giai, and P. Quentin, *Nuclear Physics* **A238**, 29 (1975).

6. Calculated using the π-N phase shift code SAID, R. Arndt, Virginia Polytechnic Institute and State University.

7. R. A. Arndt, J. M. Ford, and L. D. Roper, *Physical Review* **D32**, 1085 (1985).

8. G. Höhler, Pion Nucleon Scattering, in Landolt-Börnstein Numerical Data and Functional Relationships in Science and Technology, New Series, Vol. 9, edited by H. Schopper (Springer-Verlag, Berlin, 1983).

9. J. C. Peng, J. Kapustinsky, C. Lee, M. J. Leitch, T. K. Li, L. C. Liu, J. M. Moss, J. E. Simmons, S. M. Teng, C. Smith, and R. R. Whitney, *Physical Review Letters* **58**, 2027 (1987).

10. W. O. Lock and Measday, Intermediate Energy Nuclear Physics (Methuen and Co., Ltd., London, 1970), p. 183.

11. For a discussion, see H. A. Bethe and F. de Hoffman, *Mesons and Fields, Vol. II: Mesons* (Row, Peterson, and Co., Evanston, 1955), p. 20ff.

12. H. W. Baer, R. D. Bolton, J. D. Bowman, M. D. Cooper, F. H. Cverna, R. H. Heffner, C. M. Hoffman, N. S. P. King, J. Piffaretti, J. Alster, A. Doron, S. Gilad, M. A. Moinester, P. R. Bevington, and E. Winkelmann, *Nuclear Instruments and Methods* **180**, 445 (1981).

13. S. H. Rokni, H. W. Baer, A. G. Bergmann, J. D. Bowman, F. Irom, M. J. Leitch, C. J. Seftor, J. Alster, E. Piasetzky, B. L. Clausen, R. A. Loveman, R. J. Peterson, J. L. Ullmann, J. Comfort, J. N. Knudson, and U. Sennhauser, Los Alamos preprint LA-UR-87-303 (1987).

14. S. H. Rokni, Ph.D. dissertation, Utah State University, 1987.

15. W. B. Cottingame and D. B. Holtkamp, *Physical Review Letters* **45**, 1828 (1980).

16. H. W. Baer, J. D. Bowman, M. D. Cooper, F. H. Cverna, C. M. Hoffman, M. B. Johnson, N. S. P. King, J. Piffaretti, E. R. Siciliano, J. Alster, A. Doron, S. Gilad, M. Moinester, P. R. Bevington, and E. Winkelman, *Physical Review Letters* **45**, 982 (1980).

17. U. Sennhauser, E. Piasetzky, H. W. Baer, J. D. Bowman, M. D. Cooper, H. S. Matis, H. J. Ziock, J. Alster, A. Erell, M. A. Moinester, and F. Irom, *Physical Review Letters* **51**, 1324 (1983).

18. M. B. Johnson, in LAMPF Workshop on Pion Single Charge Exchange, January 1979, Los Alamos Scientific Laboratory report LA-7892-C, H. W. Baer, J. D. Bowman, and M. B. Johnson, Eds., p. 343.

19. M. B. Johnson, *Physical Review C* **27**, 192 (1980).

20. D. Ashery, I. Navon, G. Azuelos, H. K. Walter, H. J. Pfeiffer, and F. W. Schlepütz, *Physical Review C* **23**, 2173 (1981).

21. J. L. Ullmann, P. W. F. Alons, J. J. Kraushaar, J. H. Mitchell, R. J. Peterson, R. A. Ristinen, J. N. Knudson, J. R. Comfort, H. W. Baer, J. D. Bowman, M. D. Cooper, D. H. Fitzgerald, F. Irom, M. J. Leitch, and E. Piasetzky, *Physical Review C* **33**, 2092 (1986).

22. F. Irom, M. J. Leitch, H. W. Baer, J. D. Bowman, M. D. Cooper, B. J. Dropesky, E. Piasetzky, and J. N. Knudson, *Physical Review Letters* **55**, 1862 (1985).

23. F. Irom, H. W. Baer, A. G. Bergmann, J. D. Bowman, P. Heusi, D. H. Fitzgerald, C. J. Seftor, M. E. Sadler, J. N. Knudson, W. J. Briscoe, P. W. F. Alons, E. Piasetzky, and S. H. Rokni, *Physical Review C* (in press).

24. P. A. Seidl, M. D. Brown, R. R. Kiziah, C. F. Moore, H. W. Baer, C. L. Morris, G. R. Burleson, W. B. Cottingame, S. J. Greene, L. C. Bland, R. Gilman, and H. T. Fortune, *Physical Review C* **30**, 973 (1984).

25. K. K. Seth, M. Kaletka, D. Barlow, D. Kielczewska, A. Saha, L. Casey, D. Goodman, R. Seth, and J. Stuart, *Physics Letters* **155B**, 339 (1985).

26. C. L. Morris, S. J. Greene, R. Gilman, H. T. Fortune, J. D. Zumbro, J. A. Faucett, G. R. Burleson, K. S. Dhuga, P. A. Seidl, S. Mordechai, and C. F. Moore, *Physical Review Letters* **54**, 775 (1985); and C. L. Morris, private communication.

27. H. W. Baer, M. J. Leitch, R. L. Burman, M. D. Cooper, A. Z. Cui, B. J. Dropesky, G. C. Giesler, F. Irom, C. L. Morris, J. N. Knudson, J. R. Comfort, D. H. Wright, and R. Gilman, *Physical Review C* **35**, 1425 (1987).

28. M. J. Leitch, E. Piasetzky, H. W. Baer, J. D. Bowman, R. L. Burman, B. J. Dropesky, P. A. M. Gram, F. Irom, D. Roberts, G. A. Rebka, Jr., J. N. Knudson, J. R. Comfort, V. A. Pinnick, D. H. Wright, and S. A. Woods, *Physical Review Letters* **54**, 1482 (1985).

29. Z. Weinfeld, E. Piasetzky, H. W. Baer, R. L. Burman, M. J. Leitch, C. L. Morris, D. H. Wright, S. H. Rokni, and J. R. Comfort, Los Alamos preprint LA-UR-87-1073 (1987); also PANIC'87 loc. cit., p. 364.

30. M. J. Leitch, H. W. Baer, R. L. Burman, M. D. Cooper, B. J. Dropesky, F. Irom, C. L. Morris, J. N. Knudson, J. R. Comfort, D. H. Wright, R. Gilman, E. Piasetzky, and Z. Weinfeld (to be published).

31. A. Altman, R. R. Johnson, U. Wienands, N. Hessey, B. M. Barnett, B. M. forster, N. Grion, D. Mills, F. M. Rozon, G. R. Smith, R. P. Trelle, D. R. Gill, G. Sheffer, and T. Anderl, *Physical Review Letters* **55**, 1273 (1985).

32. A. Altman, R. R. Johnson, B. M. Barnett, N. Grion, N. Hessey, D. Mills, F. M. Rozon, G. R. Smith, M. Sevior, R. P. Trelle, U. Wienands, D. R. Gill, G. Sheffer, and T. Anderl, *Bulletin of the American Physical Society* **31**, 802 (1986).

33. DCX data compilation by R. Gilman, Ph.D. dissertation, University of Pennsylvania, 1985 (Los Alamos report LA-10524-T).

34. R. Gilman, H. T. Fortune, J. D. Zumbro, C. M. Laymon, G. R. Burleson, J. A. Faucett, W. B. Cottingame, C. L. Morris, P. A. Seidl, C. F. Moore, L. C. Bland, R. R. Kiziah, S. Mordechai, K. S. Dhuga, *Physical Review C* **35**, 1334 (1987).

35. M. B. Johnson and E. R. Siciliano, *Physical Review C* **27**, 730 (1983), and *Physical Review C* **27**, 1647 (1983).

36. S. J. Greene, C. J. Harvey, P. A. Seidl, R. Gilman, E. R. Siciliano, and M. B. Johnson, *Physical Review C* **30**, 2003 (1984).

37. G. A. Miller, *Physical Review Letters* **53**, 2008 (1984).

38. G. A. Miller, in Proceedings of the LAMPF Workshop on Pion Double Charge Exchange, January 1985, Los Alamos National Laboratory report LA-10550-C (H. W. Baer and M. J. Leitch, Eds.), p. 193.

39. W. R. Gibbs, W. B. Kaufmann, and P. B. Siegel, Workshop, loc. cit., p. 90.

40. E. R. Siciliano, Workshop, loc. cit., p. 180.

41. E. R. Siciliano, M. D. Cooper, M. B. Johnson, and M. J. Leitch, *Physical Review C* **34**, 267 (1986).

42. L. C. Liu, Workshop, loc. cit., p. 109.

43. T. Karrapiperis and M. Kobayashi, *Physical Review Letters* **54**, 1230 (1985); SIN preprint PR-85-04 (1985); and Abstract, Book I, Sixth International Conference on Particles and Nuclei, Kyoto, Japan, April 1987 (PANIC'87), p. 368.

44. G. A. Miller and J. E. Spencer, *Annals of Physics* **100**, 562 (1976).

45. L. C. Liu, *Physical Review C* **27**, 1611 (1983).

46. E. Oset and D. Strottman, *Nuclear Physics* **A355**, 437 (1981).

47. E. Oset, D. Strottman, M. J. Vicente-Vacas, Ma Wei-Hsing, *Nuclear Physics* **A408**, 461 (1983).

48. T. Karapiperis, M. Kobayashi, and M. Hirata, *Physics Letters* **144B**, 23 (1984).

49. M. B. Johnson and L. S. Kisslinger, *Physics Letters* **168B**, 26 (1986).

50. M. Bleszynski and R. Glauber, "Pion Double Charge-Exchange and Nuclear Correlations," Harvard University preprint (1987).

51. S. Cohen and D. Kurath, *Nuclear Physics* **73**, 1 (1965).

52. D. S. Koltun and A. Reitan, *Physical Review* **139**, B1372 (1965).

53. E. Bleszynski, M. Bleszynski, and R. Glauber, PANIC'87, loc. cit., p. 358.

54. W. B. Kaufmann and W. R. Gibbs, private communication, 1987; calculations are based on the theory of Ref. 44.

55. N. Auerbach, W. R. Gibbs, and E. Piasetzky, Los Alamos preprint LA-UR-86-4283 (1986); also PANIC'87, *ibid.*, p. 366.